Manuscript in preparation for *Coastal Engineering*

title: The Sum of the Parts: Green, Gray, and Green-Gray Infrastructure to Mitigate Wave Overtopping

author/affiliation:
Margaret Libby (corresponding author), Graduate Student, School of Civil and Construction Engineering, Oregon State University, 101 Kearney Hall, Corvallis, Oregon, 97331, USA. libbym@oregonstate.edu

Tori Tomiczek, Associate Professor, Naval Architecture and Ocean Engineering Department, U.S. Naval Academy, 590 Holloway Road, 11D, Annapolis, Maryland, 21402, USA. vjohnson@usna.edu

Daniel Cox, Professor, School of Civil and Construction Engineering, Oregon State University, 101 Kearney Hall, Corvallis, Oregon, 97331, USA. dtc@oregonstate.edu

Pedro Lomónaco, Director, O. H. Hinsdale Wave Research Laboratory, Oregon State University, 3550 SW Jefferson Way, Corvallis, Oregon, 97333, USA. pedro.lomonaco@oregonstate.edu

keywords:
- Coastal flood hazard mitigation
- Nature-based solutions
- Hybrid systems
- Mangroves
- Revetments
- Physical model

highlights
- Physical model study of a hybrid system with a mangrove forest and a rock revetment
- Performance parameter was the mean rate of overtopping per unit width
- A realistic mangrove forest provided overtopping protection comparable to revetment
- The hybrid system performed as a series of independent components

Abstract

Hybrid approaches to shoreline protection, where natural ("green") features are combined with hardened ("gray") infrastructure, are increasingly used to protect coastlines from erosion and flood-based hazards. Our understanding of hybrid systems is limited, and it is unknown whether the components of these systems interact in any meaningful sense to provide flood reduction benefits that are greater or less than "the sum of the parts." In this study, a large-scale physical model was used to investigate the overtopping of a vertical wall protected by a hybrid system where an idealized *Rhizophora* mangrove forest of moderate cross-shore width fronted a rubble-mound revetment. Configurations included the wall alone, the wall with a low- or intermediate-density mangrove forest without the revetment, the wall with the revetment, and the wall with an intermediate- or high-density mangrove forest and the revetment. The study isolated the reduction in overtopping of the wall by the revetment component, the mangrove forest component, and the interaction between the components of the hybrid system. The total reduction by the hybrid system was estimated within 5% accuracy as the sum of the reduction by each component minus the product of the component reductions. Comparison of the proportional reduction in overtopping by the mangrove forest on the wall alone and the wall with the revetment indicated that the mangrove forest reduced the overtopping of the revetment by approximately the same proportion that the forest reduced the overtopping of the wall. Therefore, (1) total overtopping reduction by the hybrid system was modeled as the reduction expected from the green and gray components in series. Additional analysis showed that (2) for the same wave conditions, a mangrove forest of moderate cross-shore width can have equal or greater protective benefits than a coastal revetment, (3) there is an exponential relationship between the discharge rate and the forest density, and (4) the mangrove forest, the revetment, and the hybrid system all provided greater reduction in overtopping as wave steepness increased. The tests in this study were conducted without wave breaking, with constant freeboard and water depth, with a specific revetment geometry, and without a mangrove canopy. Therefore, these results should be interpreted with caution if used for engineering design.

Keywords

Coastal flood hazard mitigation, nature-based solutions, hybrid systems, mangroves, revetments, physical model

1. Introduction

The potential for mangrove forests to mitigate coastal flooding and wave damage is well-established. Mangroves have been observed to attenuate the heights of sea and swell waves (Mazda et al., 1997; Bao, 2011) and to protect shorelines from hurricane damage while sustaining minimal damage themselves (Tomiczek et al., 2020a). Numerical model studies have shown that in cyclonic storms, mangroves attenuate wave height and storm surge and reduce sediment loss (Guannel et al., 2015, 2016; Montgomery et al., 2019). A recent coupled hydrodynamic and economic model valued the flood protection services provided by mangrove forests worldwide at more than US $65 billion annually (Menéndez et al., 2020). A cost-benefit study by Narayan et al. (2016) on natural and nature-based coastal defenses found that for the purpose of wave height attenuation, mangrove forests 800 m – 1500 m in width are several times as cost-effective as submerged breakwaters, especially in greater water depths (up to 1.8 m, within the growth limits of mangroves) where the construction costs of breakwaters increase. In addition to their flood protection services, mangrove forests offer ecological benefits including carbon storage (Alongi, 2014; Taillardat et al., 2018) and provision of critical habitat (Faunce & Serafy, 2006; Kathiresan & Bingham, 2001; Nagelkerken et al., 2008).

Laboratory studies of the engineering performance of mangrove forests have primarily considered the *Rhizophora* genus, which is found in intertidal zones of tropical regions worldwide and which is characterized by a complex root structure consisting of a network of exposed prop roots, or stilt roots, anchoring the trees in the soil (DeYoe et al., 2020). Maza et al. (2019) quantified the damping of wave height and wave forces through a small-scale physical model of a *Rhizophora* forest and found that the experimental results were well-predicted from the analytical equations of Dalrymple et al. (1984) and Mendez & Losada (2004). Tomiczek et al. (2020b) studied wave transformation through a small-scale *Rhizophora* forest and the consequent reduction in wave loads on model residential structures placed behind the forest and found that increasing the cross-shore thickness of the forest improved the wave load reduction. In an analysis of the same study, van Dang et al. (2023) found that a mangrove forest of 8.16 m cross-shore width (full-scale) reduced cross-shore velocities around model buildings and wave loads on the buildings by the same amount as a seawall or submerged breakwater. van Dang et al. (2023) further found that a mangrove forest of 19.04 m cross-shore width (full-scale) reduced cross-shore velocities around model buildings and wave loads on the buildings by the same amount as the seawall combined with the submerged breakwater. Kelty et al. (2022) constructed a full-scale model of a *Rhizophora* forest to study wave height attenuation by the mangroves. Kelty et al. (2022) found that the decay rate of the wave height doubled with the mangrove density and that the Reynolds number must be re-scaled to compare reduced-scale experiments on wave attenuation by mangroves to prototype-scale experiments. While these studies have provided detailed insights into the effects of mangrove forests on the attenuation of wave height and wave loads, laboratory research quantifying the effects of mangroves on wave overtopping of coastal infrastructure is lacking.

Wave overtopping is an important metric of effective coastal defense systems. High overtopping volumes can erode shorelines, damage structures and vessels, and threaten the safety of drivers and pedestrians on coastal roads (Franco & Franco, 1999; U.S. Army Corps of Engineers, 2002; van der Meer et al., 2018). For conventional overtopping protection structures including vertical walls and revetments, extensive field and laboratory research has been undertaken to quantify the expected overtopping discharge given specific wave conditions and structure characteristics. Empirical formulas have been developed to model the average discharge as an exponential function of the structure freeboard relative to the wave height, wave period, and/or wavelength, with coefficients given for specific structure geometries (U.S. Army Corps of Engineers, 2002). Research campaigns including OPTICREST and CLASH have synthesized physical modeling experiments, numerical simulations, and field observations of overtopping to develop rigorous datasets of overtopping measurements (De Rouck et al., 1999, 2009). The results of these experiments have informed the development of engineering guidance for overtopping protection structures, particularly the *EurOtop Manual* (van der Meer et al., 2018), which prescribes design formulas specific to structure geometry, shoreline profile, and incident wave condition. Recent investigations on overtopping have studied the thickness of the overtopping layer (Koosheh et al., 2024) and the effects of storm surge on wave overtopping (Jo et al., 2024).

While existing empirical formulas and design guidance for overtopping protection structures do not provide recommendations for designs which include natural and nature-based features (NNBF), general practice guidance on the use of NNBF for flood risk management is becoming more available. Bridges et al. (2021) recommended the use of mangroves, where ecologically appropriate, for erosion reduction, wave attenuation, and surge attenuation. Bridges et al. (2021) specified that mangrove forest widths of O(1) m – O(10) m, O(10) m – O(100) m, and O(100) m – O(1000) m, respectively, are required to achieve these engineering objectives, although the authors noted that mangrove forest widths of as little as 50 m have been observed to measurably reduce storm surge. More generally, Bridges et al. (2021) stated that wetland performance in terms of flow resistance, wave attenuation, and erosion resistance is improved by increased plant height, rigidity, and stem and root density. *Rhizophora* forests, which are characterized by tall, woody trees with dense aerial root systems, are well-suited to these performance metrics.

For systems of vegetation fields fronting a conventional hard structure, recent studies have investigated the validity of an approach where the attenuated wave height is applied to a standard formula for predicting the performance of the hard structure. In collaboration with Kelty et al. (2022), Mitchell (2021) and Tomiczek et al. (2024) measured wave forces on a vertical wall fronted by a model mangrove forest and found that the attenuated wave height at the shoreward edge of the forest could be applied to the wave force formula by Goda (2010) to accurately predict the wave force on the wall. Conversely, Maza et al. (2022) measured wave runup on a rigid planar slope fronted by model vegetation fields and found that when the attenuated wave height, calculated from the numerical model IH2VOF, was applied to the runup equations of the *EurOtop Manual* (van der Meer et al., 2018), the prediction overestimated the measured runup. Maza et al. (2022) attributed the overprediction to nonlinear interactions between the waves, the vegetation, and the slope in the physical model.

The present study utilized a large-scale physical model to investigate the overtopping performance of a hybrid system with an idealized *Rhizophora* mangrove forest seaward of a rubble-mound revetment abutting a vertical wall. The primary research objective was to determine whether the hybrid system could be treated as the linear combination of components or whether strong (nonlinear) interactions existed between components, and the components of the hybrid system were therefore tested individually and in combination. The reduction in overtopping provided by the forest was compared to that provided by the revetment, and the reduction due to the interaction between the components was quantified. Relationships between forest density and overtopping of the wall alone or the wall with the revetment were determined for the five wave conditions. The remainder of this paper is structured as follows: Section 2 describes the design of the model mangroves, the system configurations, the laboratory setup, and the tested hydrodynamic conditions; Section 3 explains the analysis of the data and presents the mean discharge rates for each wave condition and system configuration; Section 4 compares the reduction in overtopping provided by green or gray protective features, describes the behavior of the hybrid system, and shows the effects of forest density on overtopping reduction; Section 5 discusses the results of Section 4; Section 6 presents the study conclusions.

2. Physical model

2.1. Mangrove specimen

The model trees were designed and constructed by the U.S. Army Corps of Engineers for a laboratory study on wave attenuation by mangroves (Bryant et al., 2022) and were loaned to the O. H. Hinsdale Wave Research Laboratory for this study. Bryant et al. (2022) designed the models to mimic the hydrodynamic characteristics of *Rhizophora mangle*. A simplified morphology for laboratory models of *Rhizophora* sp. has been proposed by Ohira et al. (2013) and used for previous studies of wave interactions with mangroves (Maza et al., 2017, 2019; Tomiczek et al., 2020b; Kelty et al., 2022). Following the assumptions of Ohira et al. (2013), Bryant et al. (2022) modeled the tree trunk as a vertical cylinder and the tree roots as parabolic curves centered on the vertical axis of the trunk. The natural trees feature a canopy, which is not included in the model or in the design by Ohira et al. (2013). Bryant et al. (2022) justified the exclusion of the canopy citing Mazda et al. (2006), He et al. (2019), and Zhang et al. (2020) to assume that the canopy “contributes to wave attenuation only for very large inundation depths,” which were not tested in their study or in the current study. The design by Ohira et al. (2013) provides equations parameterizing the prop root system of a *Rhizophora* tree according to the tree diameter at breast height (*DBH*). Reported *DBH* for mature trees in *Rhizophora* forests ranges from 0.032 m to 0.256

m (Dawes et al., 1999; Jimenez & Lugo, 1985; Loría-Naranjo et al., 2015; Novitzky, 2010). A field study in Rookery Bay, Florida (Novitzky, 2010) reported an average *DBH* of 0.1274 m, which Bryant et al. (2022) chose as the representative tree trunk diameter. Bryant et al. (2022) developed a simplified prop root system consisting of seven symmetrical pairs of roots centered on the tree trunk and calculated the height and curvature of each root pair from Ohira et al. (2013). For the model trees, Bryant et al. (2022) scaled down the trunk diameter, root height, and root diameter by a geometric scale factor of 2.1 and oriented the root pairs around the vertical axis of the trunk at 45° intervals. The tree trunk height was chosen so that the trunk would be emergent for all wave and water depth conditions.

To reduce cost and overall complexity of the test setup, we assumed a geometrical scale of 1:2 with the prototype system used by Kelty et al. (2022). We did not attempt to model the specific material properties of mangroves, although we assumed that the bending stiffness of the PVC was sufficiently similar to that of the natural trees to model the response of the mangroves to waves (Bryant et al., 2022). We simulated the anchoring of the roots in soil by using zip ties to hold the root ends to one another or to the flume floor, which restricted movement of the roots. Table 1 lists the full-scale and model-scale dimensions of the mangrove tree models, including diameter at breast height *DBH*, trunk height h_T, and root diameter d_R. Table 2 gives the model root morphology, where the root pair height H_R is the vertical distance from the intersection of the root pair with the trunk to the bed and the root spread X_R is the horizontal distance from the center of the trunk to a root end. For comparison, the prototype-scale experiments of Kelty et al. (2022), which were conducted in the same laboratory as this study and used idealized mangroves based on Ohira et al. (2013), had trunk diameter, trunk height, root diameters, root pair heights, and root spreads twice the lengths of those used in this study.

Table 1. Mangrove model dimensions.

Parameter	Model scale (1:2) [m]	Full scale (1:1) [m]
DBH	0.060	0.121
h_T	1.524	3.049
d_R	0.016	0.032

Table 2. Mangrove model root morphology.

Root pair	Angle [°]	Model scale (1:2)		Full scale (1:1)	
		H_R [m]	X_R [m]	H_R [m]	X_R [m]
1	0	0.692	1.041	1.384	2.083
2	45	0.629	0.914	1.257	1.829
3	90	0.565	0.813	1.130	1.626
4	135	0.502	0.660	1.003	1.321
5	0	0.438	0.470	0.876	0.940
6	45	0.375	0.508	0.749	1.016
7	90	0.311	0.533	0.622	1.067

2.2. *Mangrove forest model*

Reported mature mangrove forest densities in southern Florida and the Caribbean range from 0.013 trees/m^2 to 2.02 trees/m^2 (Dawes et al., 1999; Jimenez & Lugo, 1985; Loría-Naranjo et al., 2015; Novitzky, 2010). For this study, three full-scale forest densities were considered: 0.21 trees/m^2, 0.41 trees/m^2, and 0.82 trees/m^2. This range of densities overlaps with densities tested in previous studies of wave transformation through mangrove forests (Tomiczek et al., 2020b; Kelty et al., 2022). The model-scale densities were N = 0.82 trees/m^2, $2N$ = 1.64 trees/m^2, and $4N$ = 3.28 trees/m^2. The model trees in the $4N$ forest were placed in a staggered arrangement, which was simple to construct and consistent with previous laboratory studies of mangrove forests (Maza et al., 2017, 2019; Tomiczek et al., 2020b; Kelty et al., 2022). For the $2N$ forest, half the mangroves were removed at pseudorandom from the $4N$ forest to produce an approximately uniform forest density. This procedure was repeated for the N forest.

The cross-shore width of the model forest was held constant for all densities. In natural and engineered systems, mangrove forest widths can range from O(10 m) – O(1000 m) (Macintosh, 2005; Montgomery et al., 2019; Narayan et al., 2016). Laboratory studies have primarily considered narrow and moderate cross-shore widths of 8 m – 156 m (full scale) to study flow hydrodynamics near the seaward edge of a mangrove forest (Maza et al., 2017, 2019; Tomiczek et al., 2020b; Kelty et al., 2022). For practicability and consistency with previous studies, a 19.60-m cross-shore forest width (39.20 m full-scale width) was used throughout this study. The forest width was approximately 1 – 3 times the wavelength of the incident waves. Figure 1 shows (a) a photograph of a natural *Rhizophora mangle* forest and (b) the $2N$ model forest constructed for this study.

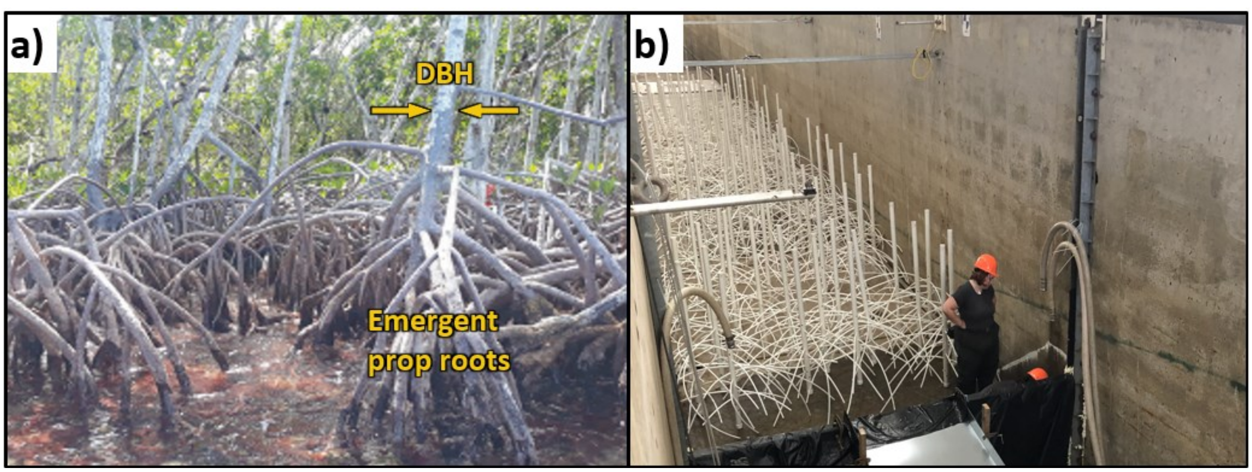

Figure 1. (a) Natural Rhizophora forest in Islamorada, FL. (b) Model forest of 2N *density in flume.*

2.3. *Configurations*

The green-gray elements of the hybrid system were tested individually and jointly with six system configurations. Figure 2 shows each configuration with a schematic drawing and a photograph in panels

(a) – (f). Figure 2 (a), (b), and (c) show the three configurations without the revetment: a wall-alone configuration and configurations with added mangrove forest densities of *N* and *2N*, respectively. Figure 2 (d), (e), and (f) show the three configurations with a revetment: a wall and revetment configuration and configurations with added mangrove forest densities of *2N* and *4N*, respectively. This matrix of configurations allowed for comparison between the performance of the individual green or gray features and the combination of features. The forest configurations, descriptions, nominal densities, number of trees N_{trees}, and densities in trees/m^2 are given in Table 3.

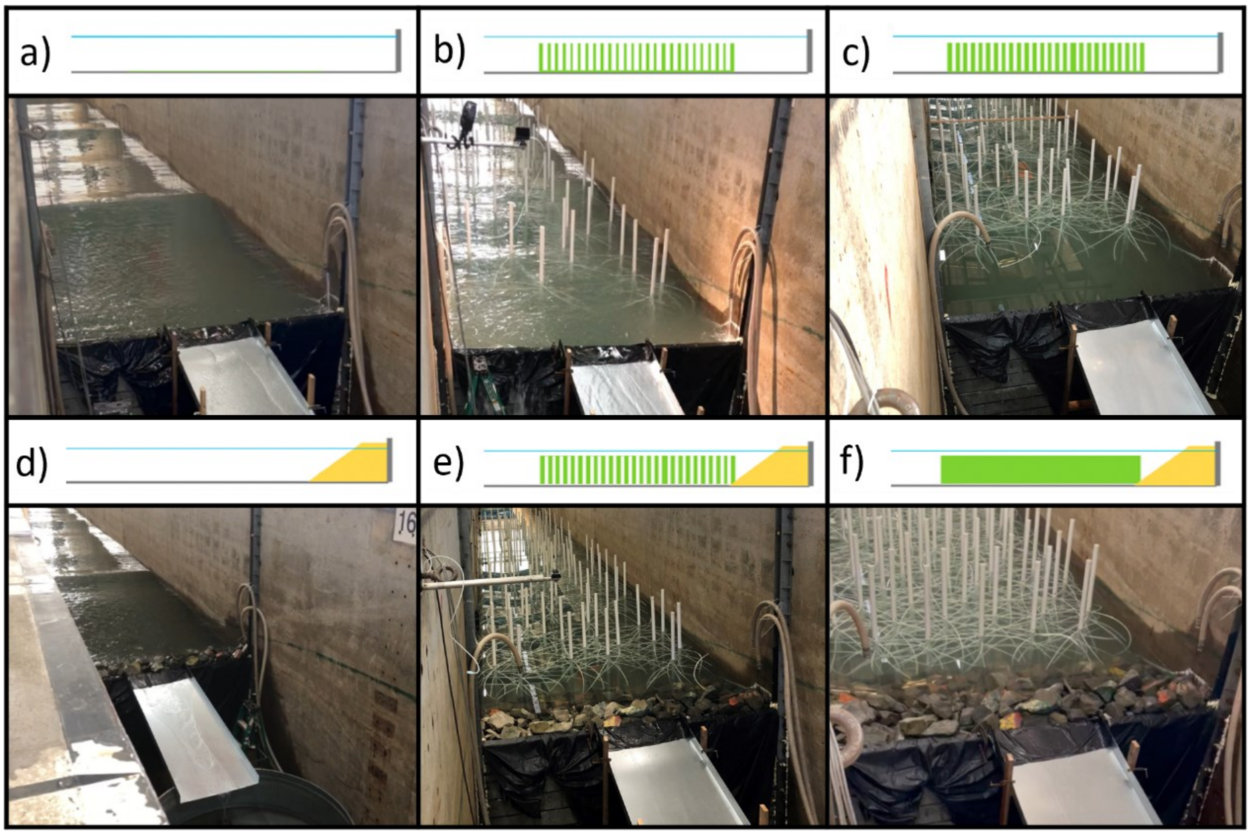

Figure 2. Configurations tested during the wave overtopping experiments. (a) Wall alone, (b) Wall + N *forest, (c) Wall +* 2N *forest, (d) Wall + revetment, (e) Wall + revetment +* 2N *forest, and (f) Wall + revetment +* 4N *forest.*

Table 3. Configurations, descriptions, and forest densities.

Configuration [-]	**Description [-]**	**Nominal density [-]**	N_{trees} **[-]**	**Density** Model scale [trees/m^2]	**Density** Full scale [trees/m^2]
A	Wall alone	0	0	0.00	0.00
B	Wall + *N* forest	N	60	0.82	0.21
C	Wall + *2N* forest	2N	121	1.64	0.41
D	Wall + revetment	0	0	0.00	0.00
E	Wall + revetment + *2N* forest	2N	121	1.64	0.41
F	Wall + revetment + *4N* forest	4N	242	3.28	0.82

2.4. Flume bathymetry and instrumentation

The overtopping experiments were conducted in the Large Wave Flume (LWF) at the O.H. Hinsdale Wave Research Laboratory at Oregon State University. The flume layout is shown in profile view in Figure 3 and in plan view (for each of the six system configurations) in Figure 4. The coordinate system used in the LWF had the x-axis positive along the length of the flume with the origin at the wavemaker, the y-axis positive across the flume toward the west side wall with the origin at the flume centerline, and the z-axis positive upward with the origin at the flume bottom. The LWF was 104.27 m long, 3.66 m wide, and 4.57 m deep and was oriented on a north-south transect. A piecewise, continuous, adjustable bathymetry consisting of 3.66 m square reinforced concrete slabs was installed on the flume floor. Each slab occupied a flume "bay" numbered 1 – 22 for reference. For this experiment, a piston-type wavemaker was positioned at the south end of the flume. The design water depth at the wavemaker was 1.60 m. A 1:12 beach slope 7.32 m in length was installed starting at x = 17.71 m (Bay 3). The slope led to a 36.59 m flat test section starting at x = 25.03 m (Bay 5), where the design depth was h_v = 0.760 m. For configurations that included the model mangroves, a 19.60 m long mangrove forest was placed from x = 39.90 m (Bay 9) to x = 59.50 m (Bay 14). An impermeable vertical wall was installed at x = 61.62 m (Bay 15) behind which overtopping water was collected and measured. The wall was lined on the seaward side with a layer of thin plastic sheeting to minimize leakage. Leakage was observed to be minimal relative to the overtopping discharge and was consistent across all overtopping tests.

For the configurations that included a rubble-mound revetment, the revetment was placed seaward of the wall and immediately shoreward of the forest with the toe at x = 59.62 m (Bay 14). The revetment was 0.85 m in height and spanned the width of the flume. The crest of the revetment was even with the crest of the wall. The median stone diameter, calculated from the Hudson (1974) formula (U.S. Army Corps of Engineers, 2002), was conservatively designed to be 0.20 m to ensure stability against the largest waves expected to propagate in the test section water depth. The crest width of the revetment was then designed to be 0.60 m, three times the median stone diameter. The design slope was 1.5H:1V.

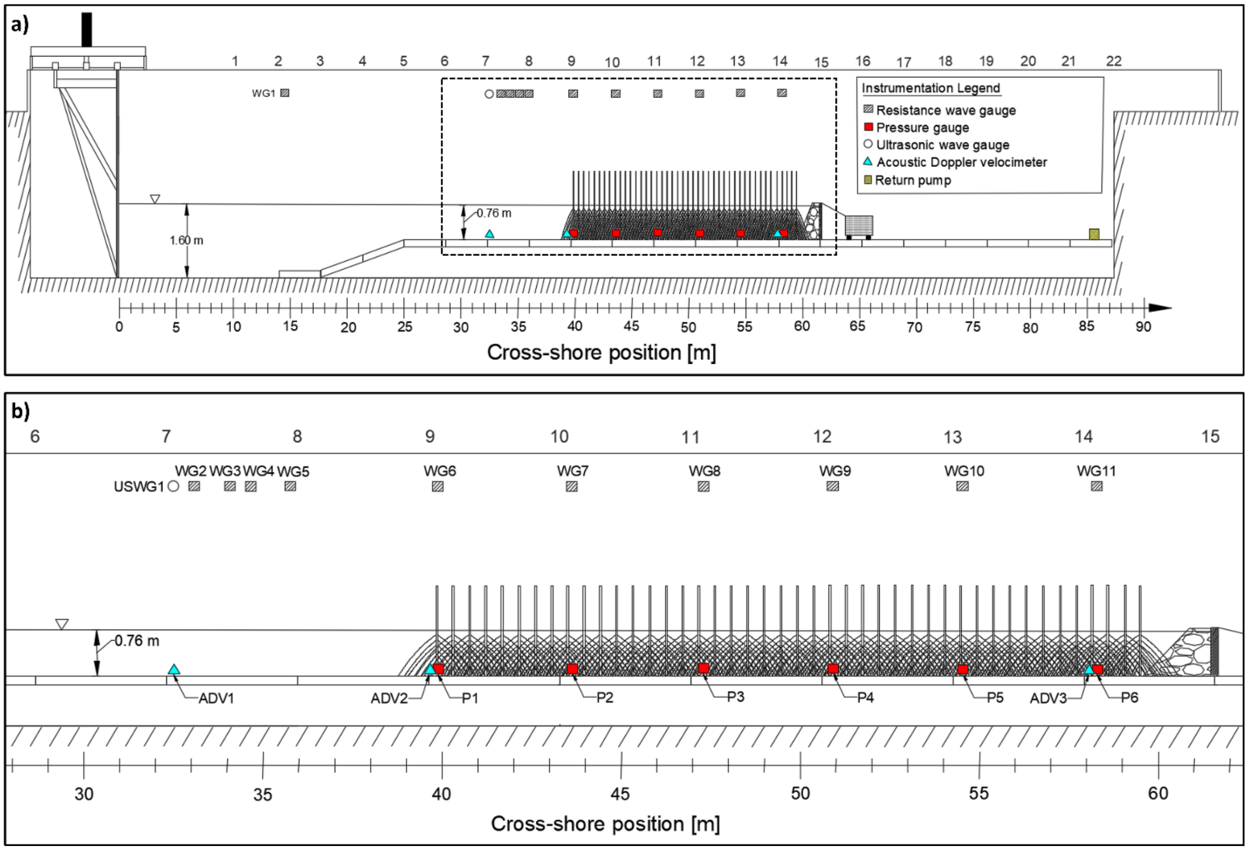

Figure 3. Bathymetry and instrumentation positions for the overtopping experiments (elevation view). System configuration shown is Configuration F with the rubble-mound revetment and the 4N *mangrove forest. (a) View of the flume from the wavemaker to the end of the flume. Vertical scale is 4x the horizontal scale. (b) Close-up view of the test section indicated by the dashed box in (a). Vertical scale is 1.6x the horizontal scale.*

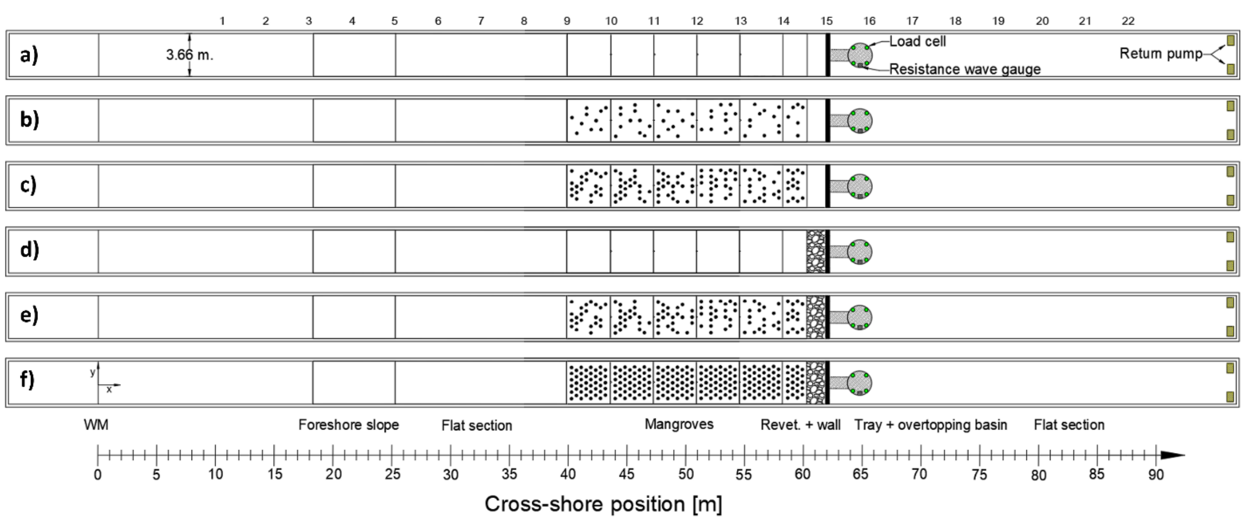

Figure 4. Plan view of flume and overtopping catchment system for the six tested configurations. From top to bottom: Configuration A (wall alone); Configuration B (wall + N *forest); Configuration C (wall +* 2N *forest); Configuration D (wall + revetment); Configuration E (wall + revetment +* 2N *forest); and Configuration F (wall + revetment +* 4N *forest). The mangrove trunks were positioned in the flume as shown in the figure.*

The *4N* forest in Configuration F was organized in 44 alternating rows of 5 and 6 trees (242 total trees placed in the flume) as shown in Figure 4. The arrangement of trees in each bay was identical. The spacing of the staggered trees in one bay of the flume, on one side of the flume centerline, is shown in Figure 5.

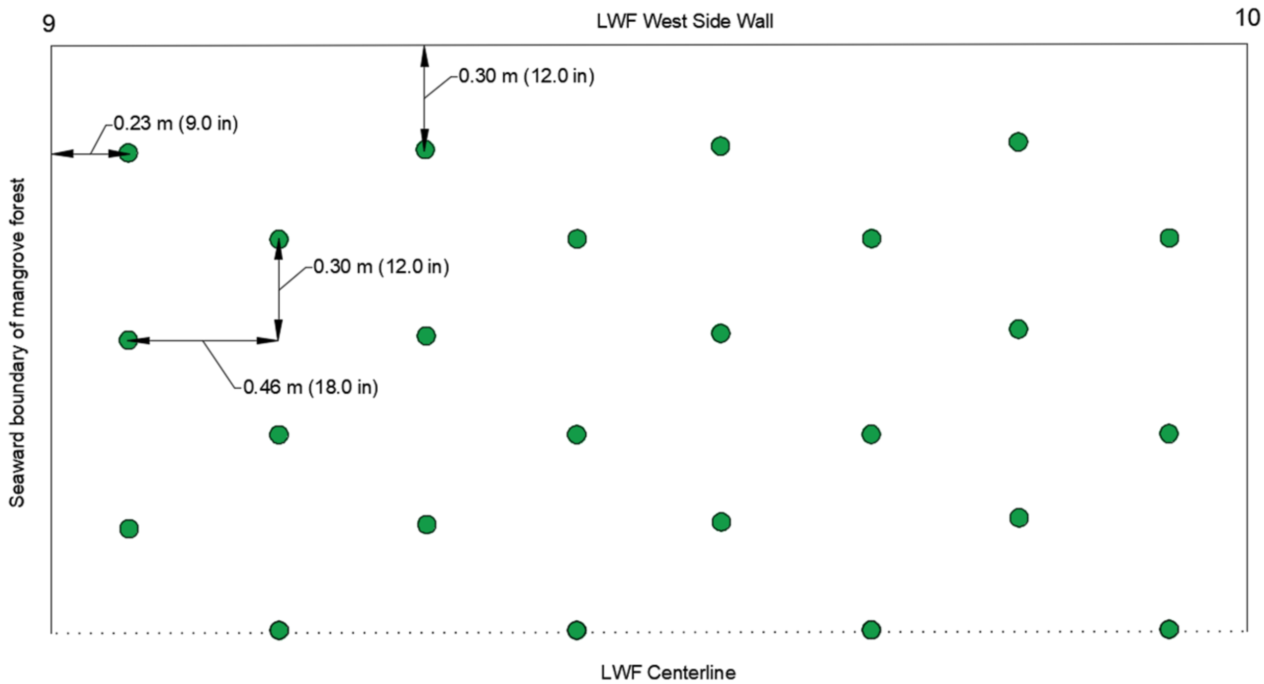

Figure 5. Spacing of model trees in the 4N *forest (plan view) for a single bay. Bay numbering is included at the top of the figure for reference. The trunks are indicated by green circles. The positioning of the trees was symmetrical about the LWF centerline, shown by the dotted line.*

Instruments including wire resistance wave gauges (WGs), acoustic Doppler velocimeters (ADVs), pressure gauges (Ps), and an ultrasonic wave gauge (USWG) were placed along the east side wall of the flume to measure the flow hydrodynamics as the waves propagated down the flume and through the model forest. The instrument locations are indicated in Figure 3 and are specified according to LWF coordinates in Table 4. The instruments were synchronized and sampled at 100 Hz. Post-processing of the raw instrument data included application of calibrations and despiking as necessary, and the post-processed data was analyzed for the results.

Table 4. Locations of instruments measuring hydrodynamic conditions in the LWF.

Instrument [-]	*x* [m]	*y* [m]	*z* [m]
WG1	14.345	-1.403	N/A
WG2	33.154	-1.365	N/A
WG3	34.063	-1.367	N/A
WG4	34.677	-1.367	N/A
WG5	35.905	-1.370	N/A
WG6	39.945	-1.411	N/A
WG7	43.607	-1.412	N/A

WG8	47.267	-1.415	N/A
WG9	50.921	-1.413	N/A
WG10	54.577	-1.408	N/A
WG11	58.242	-1.415	N/A
USWG1	32.547	-1.409	3.029
ADV1	32.549	-1.396	0.942
ADV2	39.705	-1.457	0.917
ADV3	58.040	-1.448	0.922
P1	39.945	-1.440	0.906
P2	43.608	-1.445	0.895
P3	47.266	-1.444	0.906
P4	50.922	-1.443	0.905
P5	54.591	-1.438	0.903
P6	58.254	-1.441	0.901

The overtopping catchment system shown in Figure 3 and Figure 4 consisted of a 0.993 m wide aluminum tray positioned at the center of the vertical wall to direct a portion of overtopping water into a basin. The system was similar to that used by other researchers (e.g., Franco & Franco, 1999; Bruce et al., 2009; Schoonees et al., 2021). The tray was braced by a wooden truss and held to the wall by clamps to prevent shifting or flexure of the tray as the waves overtopped the wall. The tray was not observed to obstruct the flow. A layer of thin plastic sheeting was wrapped around the end of the tray and folded over the seaward side of the wall to minimize leakage, and the sides of the tray prevented spilling as water flowed into the catchment basin. Water overtopping the wall to either side of the tray was allowed to flow freely in the area landward of the wall (Bay 15) and was pumped back to the test section during the test to minimize fluctuation in the water depth.

The catchment basin (Figure 6) was 2.32 m in diameter and 0.61 m in height. The basin rested on four load cells to measure the time-variation of the water accumulation during each test. A wire resistance wave gauge was clamped to the inside wall to measure the water surface elevation in the basin and verify the results from the load cells. The load cells and the wave gauge were synchronized with each other and with the instruments measuring hydrodynamic conditions in the flume, and all sampled at 100 Hz. A pump was placed in the basin to return the water to the test section after the completion of each test.

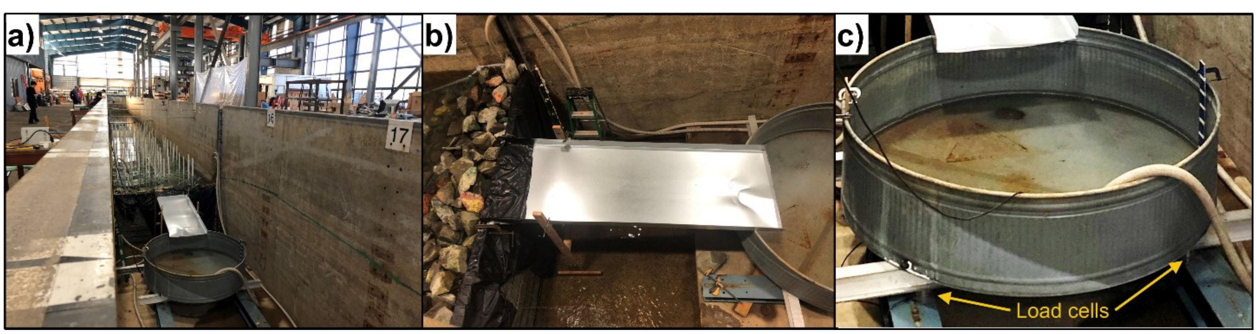

Figure 6. Overtopping catchment system. (a) View of test setup showing wavemaker (back) to overtopping basin (front). (b) Secured tray directing water into the basin. (c) Overtopping catchment basin with two of the four load cells indicated.

2.5. Hydrodynamic conditions and testing regime

The performance of the six system configurations was tested under random, regular, and transient (tsunami-like) wave regimes, and the random wave regime included conditions with one or two peaks in the wave spectrum (Libby et al., in prep.). The analysis in this paper considers the five wave conditions in the random wave regime with single-peaked energy spectra. Brief time series of free surface and corresponding wavemaker displacement were used to avoid inundation of the catchment basin. For each of the five wave conditions, approximately 1200 waves total were run across a sequence of four or seven time series including approximately 200-300 waves each. The testing regime for each wave condition was conducted according to the following procedure:

1. A TMA wave energy spectrum with peak enhancement factor $\gamma = 3.3$ was developed from the peak period and significant wave height chosen for the wave condition.
2. Four or seven time series of approximately 200-300 waves each were calculated from the TMA wave energy spectrum with an inverse fast Fourier transform algorithm implemented by the Awasys7 wave generation program (Meinert et al., 2017). The time series were calculated with distinct random seed values and were approximately equivalent in duration to one another (within the sequence).
3. The time series ("tests") were run sequentially. The catchment basin was drained between tests.
4. For consistency, the same sequences were used with Configurations A – F.

Active wave absorption, controlled by the Awasys7 wave generation program (Meinert et al., 2017), was used during the experiments. Table 5 gives the ranges of hydrodynamic conditions observed for each wave condition from the tests conducted for the six configurations. The measured hydrodynamic conditions included measured water depth h_v, the freeboard R_c between the water surface and the crest of the wall, the significant wave height H_{m0}, the peak period T_p, the number of waves observed per test N_w, and the number of tests N_{tests} conducted in sequence to reach ~1200 waves. The H_{m0} and T_p values characterized the incident waves, which were resolved with water surface elevation data from the array of wave gauges 2 – 5 (Figure 3) using the method of Zelt & Skjelbreia (1992) as implemented in the WaveLab3 desktop application (Frigaard & Lykke Andersen, 2014).

Table 5. Measured hydrodynamic conditions for overtopping tests.

Wave condition [-]	h_v [m]	R_c [m]	H_{m0} [m]	T_p [s]	N_w [-]	N_{tests} [-]
1	0.750 – 0.771	0.079 – 0.100	0.175 – 0.200	2.83 – 3.15	286 – 338	4
2	0.748 – 0.762	0.088 – 0.102	0.177 – 0.230	2.93 – 3.15	293 – 337	4
3	0.748 – 0.761	0.089 – 0.102	0.191 – 0.219	3.72 – 3.90	323 – 348	4
4	0.742 – 0.761	0.089 – 0.108	0.201 – 0.227	4.55 – 5.12	306 – 337	4
5	0.737 – 0.767	0.083 – 0.113	0.209 – 0.238	6.30 – 7.45	181 – 208	7

Table 6 lists the dimensionless parameters characterizing the wave conditions. These parameters include the relative water depth h_v/L_p, which expresses the ratio of the depth in the test section h_v to the peak wavelength L_p calculated from the peak wave period T_p using the assumptions of linear wave theory; the wave steepness, H_{m0}/L_p, which expresses the ratio of the significant wave height H_{m0} to the peak wavelength L_p; the ratio of the significant wave height H_{m0} to the water depth h_v, which is a measure of the nonlinearity of the wave; and the ratio of the model forest width L_{veg} to the peak wavelength L_p.

Table 6. Dimensionless wave parameters for overtopping tests.

Wave condition [-]	h_v / L_p [-]	H_{m0} / L_p [-]	H_{m0} / h_v [-]	L_{veg} / L_p [-]
1	0.092 – 0.105	0.022 – 0.026	0.233 – 0.262	2.42 – 2.75
2	0.093 – 0.101	0.022 – 0.029	0.233 – 0.305	2.43 – 2.65
3	0.073 – 0.077	0.019 – 0.022	0.253 – 0.289	1.92 – 2.03
4	0.055 – 0.062	0.015 – 0.018	0.267 – 0.301	1.45 – 1.65
5	0.037 – 0.044	0.011 – 0.014	0.279 – 0.322	0.98 – 1.18

The variation in significant wave height and peak period was minimal across Configurations A-F. The wave heights were approximately 0.01 m (5%) greater for the configurations with the revetment compared to configurations without the revetment, and this minor difference is not expected to affect the results. The water depth was monitored during the experiments to keep the water level constant to the extent possible. The flume was emptied and refilled each time the system configuration was changed, which introduced some variation in the water depth, and there was variation during and between the tests due to the time delay between water overtopping the wall and returning to the test section via pumps. The mean water depth for each test was determined from the mean of the water surface elevation time series reported from WG2 in the test section, and the mean freeboard was calculated as the distance between the mean water surface and the crest of the wall.

The variation in mean water level due to the overtopping and water return process was estimated from the results of a low-pass filter applied to the water surface elevation time series. The low-pass filter was applied in the time domain using a moving mean with a 60 s window. Figure 7 shows an example of the water surface elevation time series, mean water level, and the moving average. There was a slight decrease in water depth over the course of the test as the overtopping rate exceeded the rate water was returned to the test section. This reduction in water depth (0.016 m, 2.1% of the mean water depth) was characteristic of the overtopping tests. For all wave conditions, the change in the water depth over the course of each test was less than the differences in the mean depth between tests, so the depth variation during the tests did not significantly affect the results.

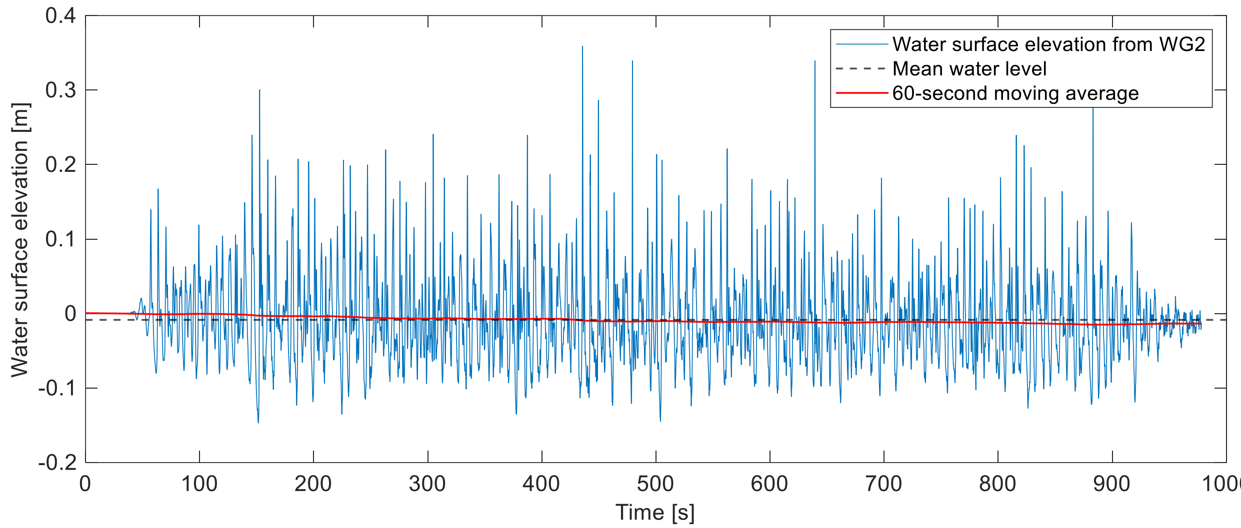

Figure 7. Water surface elevation and mean water level over the course of an overtopping test. Example shown is for the first test in the testing sequence for wave condition (5) where H_{m0} = 0.22 m and T_p = 7.1 s, and Configuration D (wall + revetment).

3. Data analysis

The overtopping discharge rates were calculated from the time series of force reported from the load cells. A time series was reported for each test in the sequence for each wave condition/system configuration combination. The force (weight) on the load cells was measured and then summed across the four load cells. The total force was then converted to volume (m^3) assuming a gravitational constant of 9.81 m/s^2 and a constant water density of 997 kg/m^3. The volume was scaled by 0.993 m^{-1} to calculate the volume of overtopping per unit width of the wall. Each time series was truncated by 80 seconds from the start and 40 seconds from the end to discount periods of the data record where overtopping did not occur due to the time delay between the starting and stopping of the wavemaker and the overtopping of the wall. For wave conditions (4) and (5) in Configuration A (wall alone), the catchment basin overflowed near the end of each test. For these tests, the end of the data record was truncated when the rate of increase in the calculated volume became zero. The truncated time series were then concatenated to produce a time series of the volume of water in the catchment basin over the test duration. A least-squares linear regression was used to calculate the overall discharge rate for the concatenated time series (Figure 8).

Figure 8 shows the concatenated time series of overtopping for Configurations A – F for wave condition (3). For wave condition (3), the overtopping volumes were approximately halved when the *N* forest (Configuration B) or the revetment (Configuration D) was installed. In other words, the forest provided the same amount of overtopping protection as the conventional revetment. The *2N* forest (Configuration C) provided significantly more overtopping protection than the conventional revetment. Further, the combination of the revetment and the *2N* mangrove forest (Configuration E) reduced the overtopping more than either the revetment (Configuration D) or the *2N* forest (Configuration C). When the revetment and the *4N* forest were installed (Configuration F), almost no overtopping occurred.

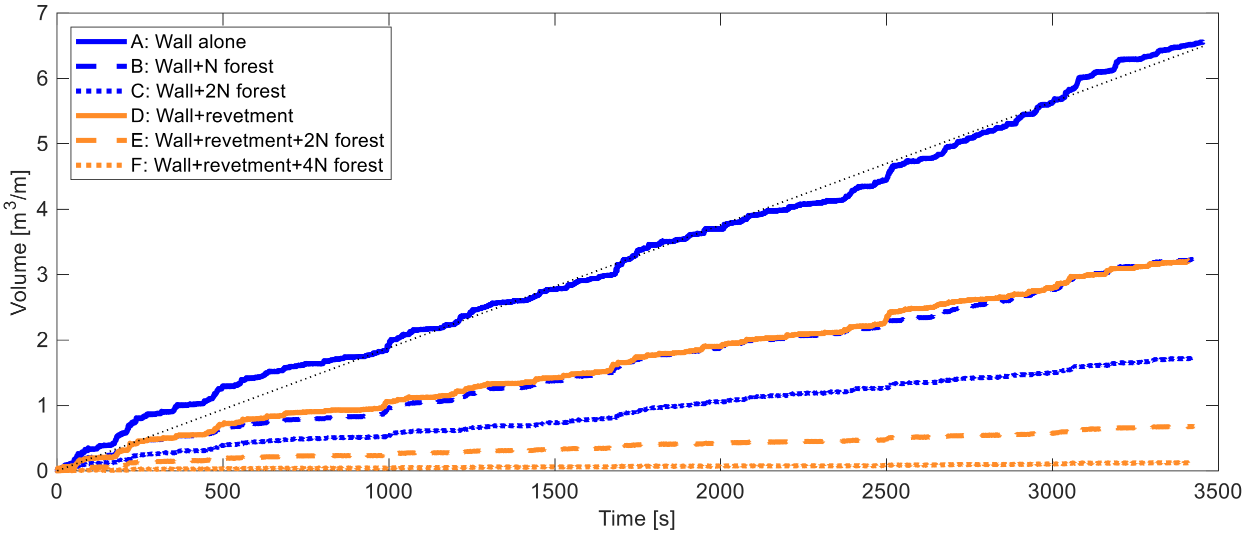

Figure 8. Time series of overtopping volumes for the six system configurations for wave condition (3). The blue curves represent configurations with no revetment, and the orange curves represent configurations with the revetment. The dotted black line shows the linear regression calculated for Configuration A. Note that Configuration B (wall + N *forest) (blue dashed curve) provided the same protection as Configuration D (wall + revetment) (orange solid curve).*

Discharge rates for all wave condition and system configuration combinations were calculated from linear regressions on the time series as shown in Figure 8. The mean r^2 value of the regressions was 0.96 with a standard deviation of 0.07. The calculated linear discharge rates were therefore considered to be sufficiently descriptive of the overtopping process, and the performance of the protective features was analyzed in terms of the reduction in discharge rate provided by each feature or combination of features.

The mean overtopping discharge rate q was compared across the 30 combinations of the five wave conditions and the six configurations (Figure 9). For each configuration, the discharge rates generally increased with increasing wave height and period. The discharge rates decreased as forest density increased for the configurations without the revetment (Configurations A – C) and for configurations with the revetment (Configurations D – F). For all wave conditions, the discharge rates for Configuration D (wall + revetment), were similar to the discharge rates for Configuration B (wall + *N* forest) and were greater than the discharge rates for Configuration C (wall + *2N* forest).

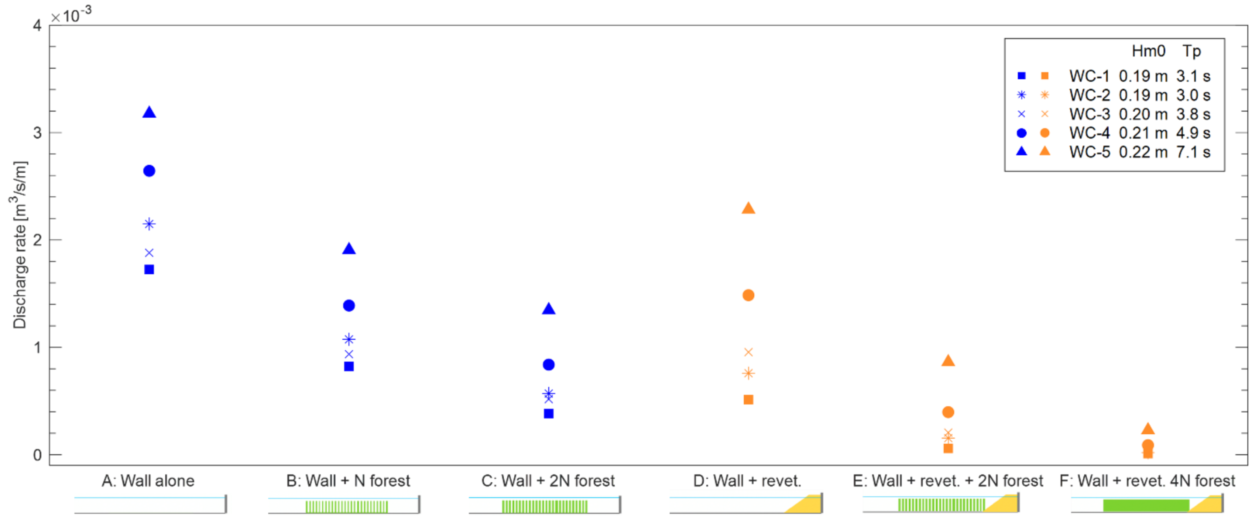

Figure 9. Discharge rates (q) calculated for each overtopping scenario. Configurations A – C, which do not include the revetment, are indicated by blue symbols, and Configurations D – F, which do include the revetment, are indicated by orange symbols. The wave conditions are indicated by the symbols as shown in the legend where e.g., "WC-1" indicates wave condition (1).

4. Results

4.1. Performance of the mangrove forest vs. the rubble-mound revetment

As shown in Figure 8, green infrastructure (mangrove forest) can provide the same wave overtopping mitigation as gray infrastructure (rubble-mound revetment) for the same water level and wave condition. This result was found consistently across the tested wave conditions. Figure 10 compares the performance of "green" and "gray" overtopping protection alternatives. In the figure, the overtopping discharge rates q_N for Configuration B (wall + N forest) are plotted against the discharge rates q_R for Configuration D (wall + revetment) for each wave condition. The discharge rates for the two configurations are very similar. The RMSE was 2.64E-4 $m^3/s/m$, approximately an order of magnitude less than the observed discharge rates. As shown in Figure 10, for wave conditions (1) and (2), which were the steepest wave conditions, the discharge for the N forest configuration was greater than that for the revetment configuration. Conversely, for wave conditions (4) and (5), which were the least steep wave conditions, the discharge for the N forest configuration was less than that for the revetment. For wave condition (3), the discharge rate was approximately identical for the N forest and revetment configurations. This is the wave condition shown in Figure 8, where the volume time series for Configuration B and Configuration D are shown by the overlapping dashed blue and solid orange curves. The wave conditions, wave steepnesses, and the absolute and percentage differences between the discharge rates for Configuration B (wall + N forest) and Configuration D (wall + revetment) are tabulated in Table 7. From the table, for most wave conditions tested here, the overtopping of the wall when the *N* forest is used for protection is essentially identical to when the conventional revetment is used for protection.

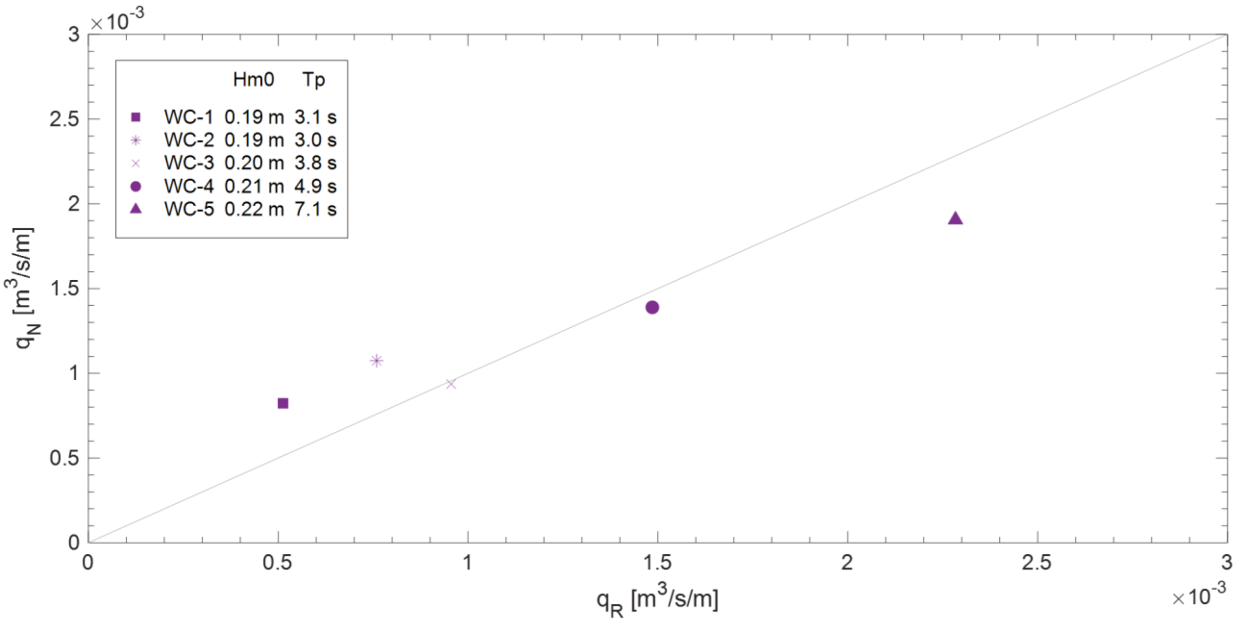

Figure 10. Overtopping discharge rates over a wall protected by Configuration B (wall + N forest), vs. discharge rates for a wall protected by Configuration D (wall + revetment). Perfect agreement is shown by the diagonal gray line.

Table 7. Wave conditions and difference in discharge rate between Configuration B and Configuration D.

Wave condition	H_{m0}	T_p	H_{m0} / L_p	q_N	q_R	$\frac{q_N - q_R}{q_R} \cdot 100$
[-]	[m]	[s]	[-]	[m³/s/m]	[m³/s/m]	[%]
1	0.187	3.06	0.024	8.23E-4	5.13E-4	60.4
2	0.193	3.03	0.025	1.07E-3	7.59E-4	41.5
3	0.203	3.84	0.020	9.36E-4	9.55E-4	-2.0
4	0.211	4.86	0.016	1.39E-3	1.49E-3	-6.5
5	0.222	7.05	0.012	1.91E-3	2.28E-3	-16.5

4.2. Performance of the hybrid system

The overtopping reduction δ_i was calculated for Configurations B through F with protective features by:

$$\delta_i = \frac{q_W - q_i}{q_W} \quad (1)$$

where q_i is the measured overtopping discharge rate for the protective configuration (e.g., q_N or q_R in Figure 10 and Table 7), and q_W is the measured discharge rate for Configuration A (wall alone). The reductions for each configuration are listed in Table 8, where the subscript *i* is replaced with *N*, *2N*, *R+2N*, and *R+4N* in reference to Configurations B through F, respectively.

Table 8. Overtopping discharge rate reduction matrix.

Wave condition	H_{m0}	T_p	H_{m0} / L_p	δ_N	δ_{2N}	δ_R	δ_{R+2N}	δ_{R+4N}
[-]	[m]	[s]	[-]	[-]	[-]	[-]	[-]	[-]
1	0.187	3.06	0.024	0.523	0.778	0.703	0.966	0.994
2	0.193	3.03	0.025	0.500	0.735	0.647	0.928	0.991
3	0.203	3.84	0.020	0.502	0.725	0.492	0.890	0.980
4	0.211	4.86	0.016	0.475	0.683	0.438	0.850	0.966
5	0.222	7.05	0.012	0.400	0.576	0.281	0.728	0.928

Table 8 shows that δ_N and δ_R are comparable for all wave conditions, which is consistent with the finding of similar q_N and q_R shown in Table 7, and which demonstrates the similar performance of the low-density *N* forest (Configuration B) and the revetment (Configuration D) for overtopping protection. As shown in the table, the intermediate-density *2N* forest (Configuration C) outperforms the *N* forest or the revetment for overtopping reduction for all wave conditions, and the hybrid system of the revetment + *2N* forest (Configuration E) outperforms the revetment or the *2N* forest alone.

Table 8 shows that while the reduction in discharge generally increases with wave steepness for all configurations, the reduction due to the revetment alone is more sensitive to the wave steepness (for the range of wave steepnesses considered here, H_{m0} / L_p ranging between 0.012 and 0.025) than the reduction due to the mangroves alone. The revetment demonstrates a reduction of 0.647 for the steepest wave condition and 0.281 for the least steep wave condition, or approximately a 57% difference in reduction. The *N* forest demonstrates a reduction of 0.500 for the steepest wave condition and 0.400 for the least steep wave condition, or approximately a 25% difference in reduction, and the *2N* forest demonstrates a reduction of 0.735 for the steepest wave condition and 0.576 for the least steep wave condition, or approximately a 20% difference in reduction. The hybrid system *R + 2N* behaves similarly to the *2N* forest, as there is a 22% difference between the reduction of 0.928 for the steepest wave condition and the reduction of 0.728 for the least steep wave condition.

The reductions δ_R, δ_{2N}, and δ_{R+2N} were compared to test the independence of the forest and revetment components of the hybrid system by equation (2):

$$\delta_{R+2N} = \delta_R + \delta_{2N} - \delta_R \delta_{2N} \quad (2)$$

where $\delta_R \delta_{2N}$ is the product of the reductions due to the individual components (see Appendix A for an explanation of the assumptions of equation (2)). We identified a bias in the relation between the observed reduction (the left-hand side, LHS, of equation (2)) and the predicted reduction (the right-hand side, RHS, of equation (2)). The bias is referred to herein as a correction factor *CF* in reduction due to the interaction between the mangroves and the revetment. The correction factor can be estimated from the RMSE between the observed data points and the predictions, which was 0.029. We developed the following relation, where $\delta_{CF} = 0.029$:

$$\delta_{R+2N} = \delta_R + \delta_{2N} - (\delta_R \delta_{2N} - \delta_{CF}) \quad (3)$$

Figure 11 compares the reduction observed for the hybrid system (LHS of equations (2) and (3)) to the prediction of equation (2) and the corrected prediction of equation (3). Conceptually, in equation (2), all reduction in overtopping due to interaction is subtracted from the prediction, while in equation (3) some reduction due to interaction is restored to the prediction. The value of the correction factor δ_{CF} is more than an order of magnitude less than the values of δ_R, δ_{2N}, and $\delta_R\delta_{2N}$ for the five wave conditions.

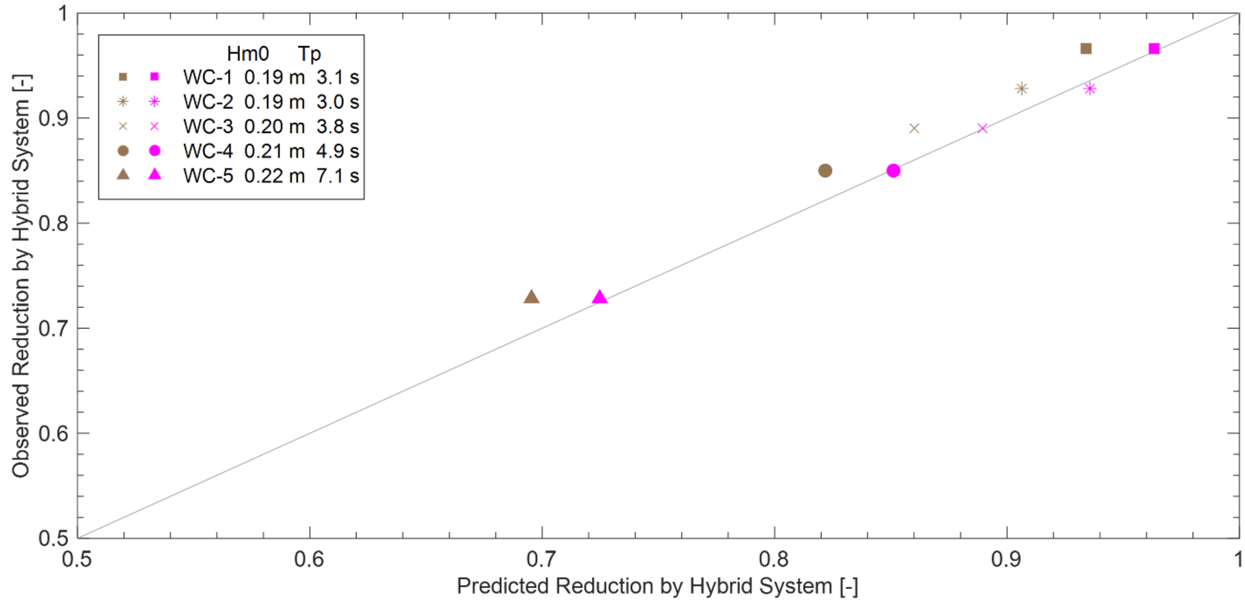

Figure 11. Comparison of observed and predicted reduction in overtopping by the hybrid system. The observed δ_{R+2N} *is plotted vs. the RHS of equation (2) by the brown points and vs. the RHS of equation (3) by the magenta points. Perfect agreement between observations and predictions is shown by the gray diagonal line.*

In a hybrid system where the components perform independently, the proportional reduction in overtopping by the *2N* forest for the wall alone should be identical to the proportional reduction by the *2N* forest for the wall with the revetment. In other words, the reduction in discharge rates from Configuration A to C, both shown in blue in Figure 9, should be the same proportion as the reduction in discharge rates from Configuration D to E, both shown in orange in the figure. To test whether this is true, we developed the equality shown by equation (4):

$$\frac{q_R - q_{R+2N}}{q_R} = \frac{q_W - q_{2N}}{q_W} \tag{4}$$

from algebraic manipulation of equations (1) and (2). Including the correction factor from equation (3) led to equation (5):

$$\frac{q_R - q_{R+2N}}{q_R} = \frac{q_W - q_{2N}}{q_W} + \frac{\delta_{CF}}{1 - \delta_R} \tag{5}$$

The development of equations (4) and (5) is shown in Appendix A.

Figure 12 compares the observed reduction by the *2N* forest for the revetment (LHS of equations (4) and (5)) to the prediction of equation (4) and the corrected prediction of equation (5), where $\delta_{CF} =$

0.029 as discussed previously. There were errors of 6.9% – 12.2% between the predictions of equation (4) and the observations, and there were errors of 0.2% – 2.7% between the corrected predictions of equation (5) and the observations.

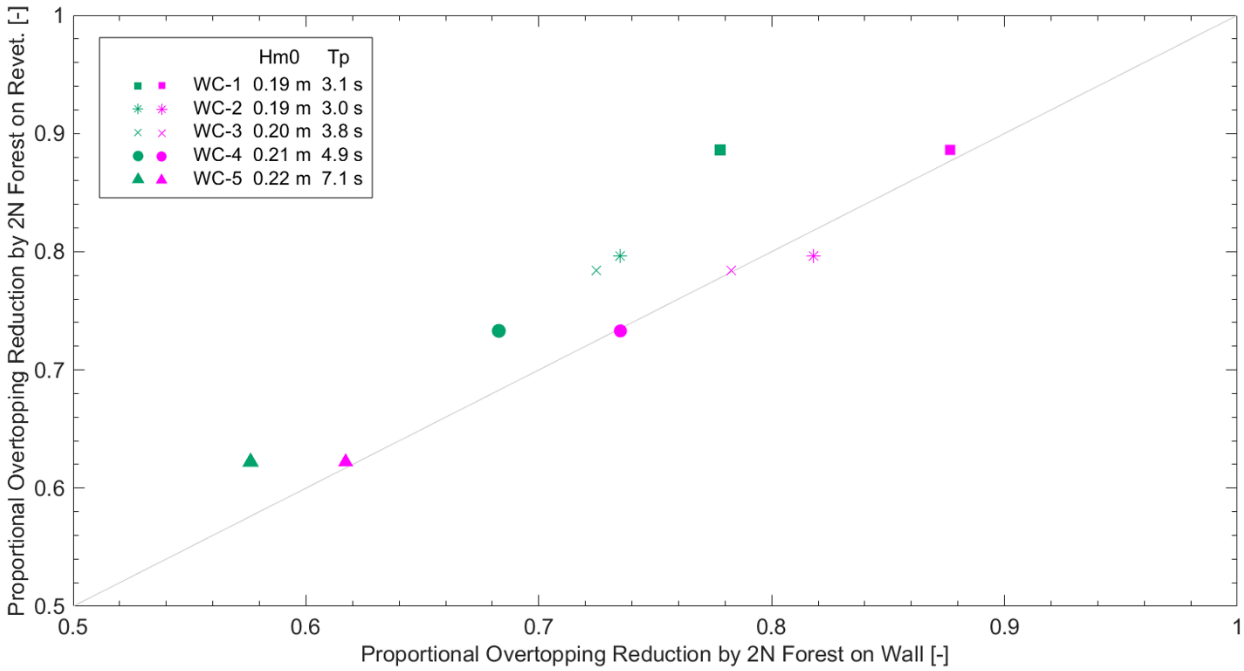

Figure 12. Observed vs predicted reduction in overtopping by the 2N *forest for the revetment. The observations are plotted vs. the prediction of equation (4) by the green points and vs. the corrected prediction of equation (5) by the magenta points. Perfect agreement between observations and predictions is shown by the gray diagonal line.*

The formulation of equation (5) shows that for the model forest and wave conditions considered in this experiment, there is a nonlinear interaction between the waves, the forest, and the revetment, where the reduction by the forest of the overtopping of the revetment (LHS of equation (5)) increases with the amount of overtopping reduction the revetment provides for the wall (δ_R). Table 9 lists the values of the terms of equation (5) for each wave condition, and the values in parentheses show the normalization by the LHS of equation (5). The table shows that for all tested wave conditions, the nonlinear interaction term is approximately an order of magnitude less than the other terms in the equation. The nonlinear interaction term depends on δ_R, which in turn depends on the wave steepness (included in Table 9) as discussed previously. Consistent with previous results showing that the reduction in overtopping by the revetment increases for steeper waves, the nonlinear interaction term increases with wave steepness.

Table 9. Reduction in overtopping of the revetment or the wall by the *2N* forest for the five wave conditions tested. Values in parentheses indicate normalization of term by LHS of equation (5).

Wave condition	H_{m0} / L_p	$\frac{q_R - q_{R+2N}}{q_R}$	$\frac{q_W - q_{2N}}{q_W}$	$\frac{\delta_{CF}}{1 - \delta_R}$
[-]	[-]	[-]	[-]	[-]
1	0.024	0.886 (1)	0.778 (0.88)	0.099 (0.11)
2	0.025	0.797 (1)	0.735 (0.92)	0.083 (0.10)
3	0.020	0.784 (1)	0.725 (0.92)	0.058 (0.07)
4	0.016	0.733 (1)	0.683 (0.93)	0.052 (0.07)
5	0.012	0.622 (1)	0.576 (0.93)	0.041 (0.07)

4.3. Effects of vegetation density

The effect of forest density on the overtopping discharge rate was investigated separately for the configurations without the revetment and the configurations with the revetment. The discharge rates q_i observed for Configurations A – C (all without the revetment) were normalized by the discharge rate q_W for Configuration A (wall alone). Figure 13 shows the normalized discharge rates and forest densities for the configurations without the revetment. Best-fit curves relating the normalized discharge rates to the vegetation densities were calculated with exponential regressions using the method of least squares and are shown on the figure. Normalized discharge rates were additionally calculated for a hypothetical *4N* forest placed in front of the wall without the revetment. The *4N* discharge rates were extrapolated using equations (1) and (3) with the discharge rates for Configuration D (wall + revetment) and the discharge rates for Configuration F (wall + revetment + *4N* forest). Error between the normalized discharge rates and the best-fit curves was minimized when $\delta_{CF} = 0.015$ in equation (3) for the extrapolated discharge rates. The extrapolated discharge rates are included on the plot to show that equations (1) and (3) predict discharge rates which are consistent with the observed data.

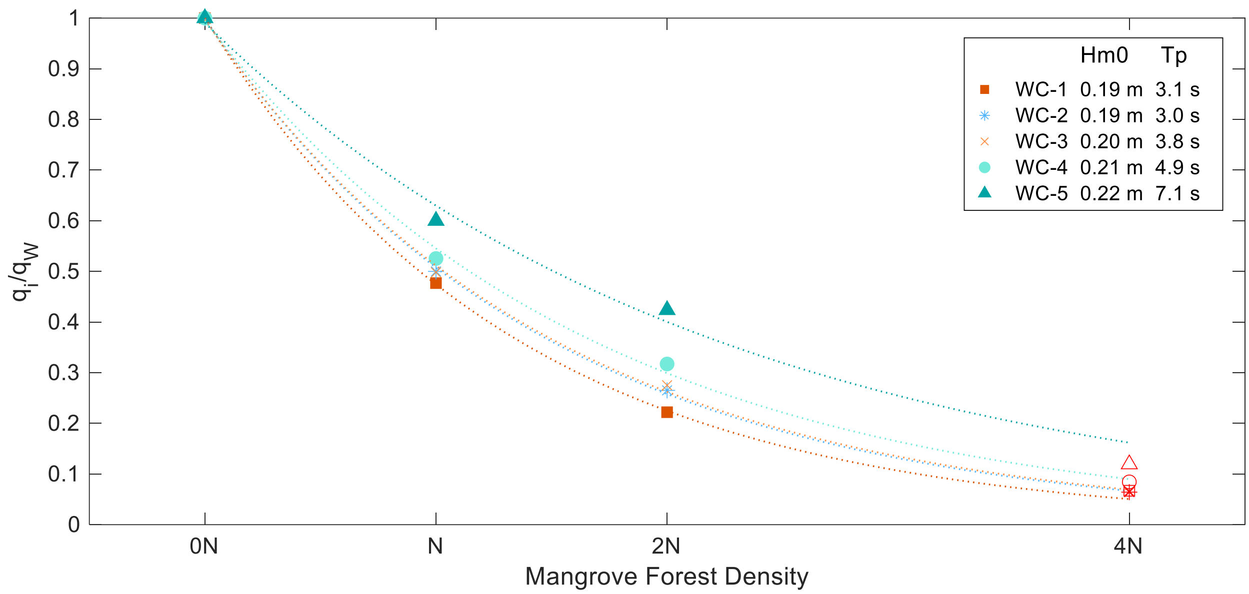

Figure 13. Overtopping discharge rate (normalized by the discharge rate for the wall alone) vs. forest density. The configurations considered here do not include the revetment. Best-fit curves (dotted) are also shown. The extrapolated values for a configuration with a 4N *forest without the revetment are shown by red open symbols.*

The discharge rates q_i observed for Configurations D – F with the revetment were normalized by the discharge rate q_R for Configuration D (wall + revetment). Figure 14 shows the normalized discharge rates and forest densities for the configurations with the revetment. Best-fit curves relating the normalized discharge rates to the vegetation densities were then calculated with exponential regressions using the method of least squares and are shown on the figure. Normalized discharge rates were additionally calculated for a hypothetical *N* forest placed in front of the wall with the revetment. The *N* discharge rates were extrapolated using equations (1) and (3) with the discharge rates for Configuration D (wall + revetment) and the discharge rates for Configuration B (wall + *N* forest). Error between the normalized discharge rates and the best-fit curves was minimized when $\delta_{CF} = 0.025$ in equation (3) for the extrapolated discharge rates. The extrapolated discharge rates are included on the plot to show that equations (1) and (3) predict discharge rates which are consistent with the observed data.

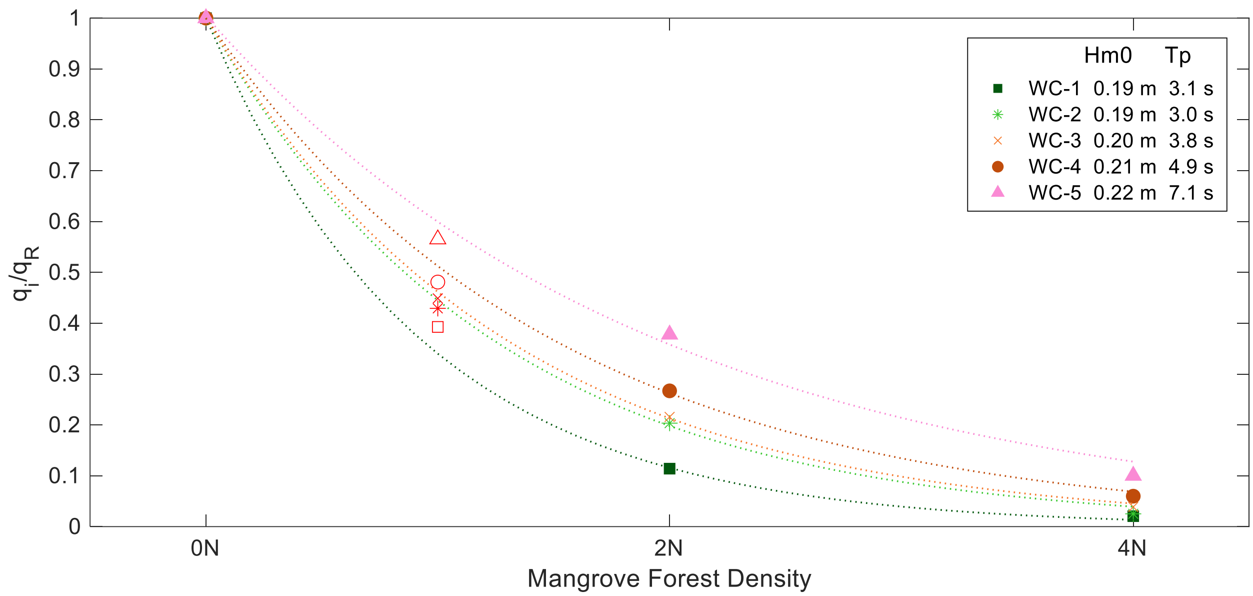

Figure 14. Overtopping discharge rate (normalized by the discharge rate for the wall + revetment) vs. mangrove forest density. The configurations considered here all include the revetment. Best-fit curves (dotted) are also shown. The extrapolated values for a configuration with an N *forest and the revetment are shown by red open symbols.*

The exponential curves shown in Figure 13 and Figure 14 take the form $f(\alpha) = q_0 e^{-\beta n}$, where *n* is the forest density multiplier on *N*, i.e., in the experiment, $n \in \{0, 1, 2, 4\}$. Since the discharge rates were normalized by the discharge rates for the unforested configurations, $q_0 = 1$ for all the calculated exponential regressions. The β decay coefficients for the wall (no revetment) configurations and the revetment configurations are tabulated in Table 10. The r^2 value exceeded 0.99 for all regressions.

Table 10. Decay coefficients for normalized discharge in systems with increasing vegetation density.

Wave condition [-]	H_{m0} [m]	T_p [s]	H_{m0} / L_p [-]	β_W [-]	β_R [-]
1	0.187	3.06	0.024	0.75	1.08
2	0.193	3.03	0.025	0.68	0.81
3	0.203	3.84	0.020	0.67	0.77
4	0.211	4.86	0.016	0.60	0.67
5	0.222	7.05	0.012	0.45	0.52

5. Discussion

5.1. Overtopping protection provided by mangrove forest

The results of this study offer a direct comparison of the overtopping protection provided by a mangrove forest and a rubble-mound revetment. For the 19.60 m model forest width (39.20 m full-scale width) considered in this study, the reduction in overtopping discharge rates from the *N*-density mangrove forest equaled or exceeded the reduction in discharge from the revetment for all but the steepest wave conditions tested (Table 8). The reduction in overtopping discharge rates from the *2N*-density mangrove forest significantly exceeded the reduction in discharge from the revetment for all the wave conditions tested (Table 8). This result shows that a mangrove forest can provide the same or greater amount of overtopping protection as a conventional rubble-mound revetment.

Further, the widths of mangrove forests in natural and engineered systems are frequently greater than the full-scale width of the model forest in this study. Typical forests widths range from tens of meters to kilometers (Bridges et al., 2021; Macintosh, 2005; Montgomery et al., 2019; Narayan et al., 2016). It is well-established that mangrove forests of greater widths attenuate waves and surge more effectively (Bao, 2011; Bridges et al., 2021), and it is therefore plausible that an *in-situ* mangrove forest of typical width would reduce overtopping of a vertical wall far more than a conventional rubble-mound revetment. It is important, however, to account for the vulnerability of mangroves to environmental stressors such as disease, drought, flood, soil erosion, and storm wind loading (Jimenez & Lugo, 1985; Doyle et al., 1995; Sippo et al., 2018; Herrera-Silveira et al., 2022; Ostrow & Cox, in review) when considering a mangrove forest as an alternative or supplement to a conventional structure.

5.2. Modeling the relationship between the components of the hybrid system

The hybrid system is modeled as a series of components which act independently, i.e., the revetment reduces overtopping of the wall by an amount δ_R, and the *2N* forest reduces overtopping of the wall by an amount δ_{2N}. The total reduction provided by the components in series is the sum of the component reductions minus the product of the reductions as shown by equation (2). The product is subtracted so the reductions by the independent components are not double-counted. Thus the performance of the hybrid system is equal to "the sum of the parts." This model predicts the performance of the hybrid system to within 5% accuracy. Rearrangement of equation (2) to equation (4) shows that the 2N forest reduces the overtopping of the vertical wall by the same proportion (within approximately 10% error) as the 2N forest reduces the overtopping of the revetment. In other words, the effects of the mangrove forest on the wall and the revetment are approximately equivalent. We caution that this relationship was observed only for overtopping reduction factors in the range 0.28 – 0.99 (Table 8), and it is unknown whether the relationship can be applied to overtopping reduction factors greater than 1 due to a feature which increases the wave overtopping.

The small, systematic error in this model of independent components was quantified as a correction factor. The correction factor represents the additional reduction in overtopping contributed by the hybrid system which is not anticipated by the independent performance model of equation (2) and equation (4). We assume that there is some interaction between the waves, the vegetation, and the structure causing this additional reduction. The study was focused on engineering performance rather than flow processes, and we did not identify the specific physical processes of such an interaction. It is possible that the process of wave reflection from the revetment and the subsequent attenuation of the reflected wave by the mangroves lead to the additional reduction. We note that the additional reduction is consistent across all wave conditions (Figure 11), suggesting that wave properties alone do not account for this correction factor. We also note that since the additional reduction (quantified as the correction factor) is an order of magnitude smaller than the reduction attributable to the mangrove forest or to the revetment (Table 9), neglecting the correction factor would be a reasonable, conservative choice for design.

5.3. Previous studies of independence in hybrid systems

The results of this study are consistent with the results reported by Tomiczek et al. (2024) in their physical model study of wave force reduction due to mangrove sheltering. Tomiczek et al. (2024) found that when measured wave conditions shoreward of the mangrove forest were used as inputs to the analytical method of Goda (2010) for determining wave forces on vertical caissons, the predictions were in good agreement with the observed 1/250th characteristic nonbreaking wave force on a vertical wall for random wave conditions, but the predictions generally overestimated the force, i.e., was conservative for design. This result suggests that interactions between the waves, the mangrove forest, and the wall have a small effect on wave forces which can be ignored for a conservative design estimate. In a physical model study of wave runup on a planar slope fronted by a mangrove forest or a salt marsh, Maza et al. (2022) found that combining numerical model predictions of wave attenuation with the runup formulas from the *EurOtop Manual* overpredicted the observed runup. In contrast to the conclusions of Tomiczek et al. (2024), Maza et al. (2022) concluded that combining the wave attenuation estimates with the runup equations did not provide a good estimate of runup, and that the interactions between the waves, the vegetation, and the slope had a significant effect on wave runup. It is possible that the significance of the interactions depends on the performance metric or on variables that were not parameterized in this experiment, such as structure freeboard or forest width.

5.4. Effects of wave steepness on overtopping

This study demonstrated that the revetment reduced the overtopping discharge rate of a vertical wall by a significantly greater amount for the steeper wave conditions than for the less steep wave conditions tested. This result is consistent with results of studies showing that runup on rubble-mound revetments increases with the Iribarren number, or the ratio of the structure slope to the square root of the wave steepness (Ahrens & Heimbaugh, 1988; U.S. Army Corps of Engineers, 2002; van der Meer et al., 2018). Since overtopping of a revetment occurs when the runup exceeds the revetment crest elevation, it is to be expected that as the runup of steep waves on the revetment is impeded, the overtopping discharge rate will be reduced. The reduction in discharge rates due to the mangrove forests were likewise observed to increase with increasing wave steepness (Table 8), and the rates of decay in the exponential relationships between vegetation density and discharge (Table 10) generally increased with wave steepness. These results are consistent with positive correlations between wave steepness and wave height decay that have been found in physical model studies of flexible vegetation (Wu & Cox, 2015) and *Rhizophora* (Maza et al., 2019). It is apparent, however, that the reduction in discharge rate due to mangrove forests is less dependent on the steepness of the wave condition than the reduction due to the rubble-mound revetment. Further, the relationship between the wave steepness and the discharge reduction by the hybrid system *R+2N* appears to be controlled by the forest component of the system, since the relationship is more similar to that for the *2N* forest than for the revetment. There is little variation with steepness for the reduction due to the *4N* forest with the revetment or for the reduction due to the hypothetical *4N* forest without the revetment, since for both systems there is very little overtopping for any wave condition. In general, it appears that a mangrove forest can serve to mitigate overtopping by longer, less steep waves which might not be impeded by a rubble-mound revetment.

5.5. Effects of vegetation parameters on overtopping

From this study, the relationship between the overtopping of a wall or revetment and the vegetation density appears to be exponential, which shows the importance of natural variation in mangrove forest density (Dawes et al., 1999; Jimenez & Lugo, 1985; Loría-Naranjo et al., 2015; Novitzky, 2010) for overtopping mitigation performance. This result concurs with the results of a recent numerical study on overtopping mitigation from a rigid cylinder array (Zhao et al., 2022). The numerical investigation by Zhao (2022) also showed that the relationship between overtopping volume and proportion of a unit volume of water occupied by vegetation remains unchanged whether the volume of vegetation is controlled by specimen diameter or vegetation density. Further, the wave height attenuation equation of Mendez & Losada (2004) implies that the wave height reduction is affected equally by vegetation density, specimen diameter, and vegetated domain cross-shore width, i.e., any one of these parameters can be increased or decreased and the resulting attenuation is the same regardless of which parameter is changed. The present study considered only a few mangrove forest densities and was restricted to a single model tree morphology and a single forest cross-shore width, so a parametric relationship combining the tree morphology, tree density, and forest width to predict the overtopping of a system with a mangrove forest cannot be developed from the results.

5.6. Characteristics of the mangrove forest model

The forest model in this study involved various forest densities (*N*, *2N* and *4N*) with a constant tree morphology for all densities. In a living mangrove forest, there are ecological controls relating the stem density and stem diameter at breast height (*DBH*), where the mangrove forest self-thins as the trees mature and the average *DBH* of the forest increases (Pranchai, 2017). Ostrow (2023) combined data from several field studies to develop allometric relations between morphological parameters of *Rhizophora sp*. The full-scale density of the *N* forest in the present study is approximately the mean density predicted from the full-scale *DBH* by Ostrow (2023), and the full-scale density of the *2N* forest is approximately at the upper limit of the 95% confidence interval of the prediction. The density of the *4N* forest is outside the predicted range, meaning it is unlikely that a natural forest of the full-scale *DBH* used in the experiment would exhibit such a high tree density. However, the model trees do not include secondary and tertiary roots, which are present in natural mangroves, so the *4N* forest may be a useful representation of root density in a natural forest. Regardless, the *4N* forest model illustrates the effect of increasing mangrove forest density on the wave overtopping of the system.

5.7. Study limitations and future research

This study was designed to test the engineering performance of the mitigation features. The investigation did not attempt to characterize the interactions between the waves and the components of the hybrid system, and the results do not provide a basic explanation for the physical circumstances where the hybrid system exceeds the expected performance due to the components. Further experimental and numerical investigations are necessary to explore these processes in more detail.

This study is additionally limited by the parameter space. The cross-shore width of the vegetation, the stem diameter of the mangroves, the structure freeboard, and the slope and porosity of the revetment are all critical parameters which were held constant in this experiment, but which are expected to significantly affect overtopping discharge rates if varied. Overtopping discharge rates are expected to decrease with increasing forest cross-shore width, increasing stem diameter, and increasing structure freeboard (Mendez & Losada, 2004; van der Meer et al., 2018). We speculate that in the hybrid system, the additional reduction due to component interactions (the correction factor) will decrease with increasing forest density or cross-shore width, increasing stem diameter, or increased structure freeboard, because small effects of interactions will become less significant compared to the increased performance of the components. A numerical modeling campaign would be useful for expanding the parameter space and exploring these possible outcomes.

The wave conditions tested in this study were designed to be nonbreaking in order to simplify the analysis; however, wave breaking is to be expected in nearshore environments where mangrove forests grow. Recent laboratory studies on mangroves have generally considered only nonbreaking wave conditions, and it is well worth investigating mangrove performance in wave energy dissipation, wave force, and wave overtopping in the context of wave breaking. It is unclear how wave breaking would influence the independent performance of green and gray components as observed in this study. However, characterizing system performance under critical or breaking wave conditions is important for informing the successful design and implementation of hybrid systems.

Furthermore, natural systems can experience wave conditions which exhibit multiple spectral peaks. The present study considered only random waves with single-peaked wave spectra. The experimental dataset includes tests performed with random waves with double-peaked wave spectra, and analysis of those tests can provide insight into the effects of low-frequency wave components on overtopping and the independent performance of the green and gray components in a hybrid system.

In addition to the analysis described in the present study, the experimental dataset offers an opportunity to test empirical and numerical approaches to the design of hybrid systems for wave overtopping. A potentially useful design approach is to use empirical wave dissipation formulas (e.g., Mendez & Losada, 2004) with the mangrove forest and apply the results as inputs to empirical formulas for wave overtopping (e.g., van der Meer et al., 2018). The results of the present study offer preliminary evidence supporting this method, but the accuracy of the method has not yet been quantified, and a recent study by Maza et al. (2022) concluded that calculations of wave dissipation cannot be used with empirical formulas from EurOtop (van der Meer et al., 2018) to predict wave runup. Alternatively, phase-averaged models (e.g., XBeach) or computational fluid dynamics models (e.g., OpenFoam) may provide more accurate predictions of overtopping and more detailed insights to the flow processes taking place in the system. An investigation comparing these methods is a logical next step in the study of hybrid systems.

6. Conclusions

This study constructed a near-prototype physical model of overtopping protection systems consisting of a rubble-mound revetment, a mangrove forest, or the hybrid system of a revetment and a mangrove forest. The experiment considered three different forest densities, where the intermediate forest density was tested in without-revetment and with-revetment configurations, and five random wave conditions where the wave steepness varied between 0.012 and 0.025. We developed a database of overtopping discharge rates for 30 combinations of wave condition and green/gray infrastructure configuration. From the study, we concluded the following:

1. The moderate-width mangrove forest of the lowest forest density provided reduction in the overtopping discharge rate of a vertical wall comparable to the reduction provided by a conventional rubble-mound revetment. This forest density was a realistic representation of a natural mangrove forest. For the steepest wave conditions, the revetment reduced the overtopping more than the mangrove forest, but for the less steep wave conditions, the forest reduced the overtopping more than the revetment. When the forest density was doubled to a density that was still a realistic representation of a natural forest, the forest reduced the discharge rate significantly more than the revetment for all wave conditions.
2. For the hybrid system consisting of a mangrove forest and a revetment placed in series, independent performance of the components is a reasonable and conservative assumption. The observed reduction in discharge provided by the hybrid system was estimated as the sum of the reduction from each component minus the product of the reduction from each component. Furthermore, the reduction in discharge provided by the mangrove forest for the wall with the rubble-mound revetment could be approximated by the reduction in discharge provided by the mangrove forest for the wall alone.
3. The estimate for the reduction in discharge provided by the hybrid system *R+2N* was improved by the inclusion of a correction factor which was an order of magnitude smaller than the other terms in the equation. Without the correction factor, the estimate underpredicted the reduction in discharge by less than 5%. The correction factor also improved the estimate of how the mangrove forest reduced the overtopping of the revetment. Without the correction factor, the estimate underpredicted the reduction in overtopping of the revetment by approximately 10%. The low magnitudes of these errors support the conclusion of independent performance of the components.

4. Increasing the density of the mangrove forest had an exponential effect on the discharge rate of a vertical wall with or without a revetment. Regardless of whether the revetment was included in the system, the rate of exponential decay increased with the wave steepness.

Quantifying the engineering performance of natural and hybrid coastal protection systems, which mitigate coastal flood hazards and provide concomitant ecological services such as habitat and carbon storage, is an essential research task. The results of the present study indicate that the "whole (green-gray system) is equal to the sum of the (green and gray) parts," and that this equality is somewhat conservative by about 5% to 10%. As discussed in Section 5.7, additional work must take place before this result should be implemented in practice.

CRediT authorship

Margaret Libby: Methodology, Validation, Formal analysis, Investigation, Data curation, Writing – original draft, Writing – review and editing, Visualization. **Tori Tomiczek**: Conceptualization, Methodology, Investigation, Data curation, Writing – review and editing, Supervision, Project administration, Funding acquisition. **Daniel Cox**: Conceptualization, Methodology, Investigation, Writing – review and editing, Supervision, Project administration, Funding acquisition. **Pedro Lomónaco**: Methodology, Investigation, Resources, Data curation, Writing – review and editing, Supervision.

Conflict of interest

The authors declare that they have no known competing financial interests or personal relationships that could appear to have influenced the work in this paper.

Data availability

The experimental data are available upon request and will be made available on the DesignSafe Data Depot at https://www.designsafe-ci.org/data/browser/public/.

Acknowledgments

The authors thank the O.H Hinsdale Wave Research Laboratory staff Tim Maddux and Rebekah Miller. We are grateful to Duncan Bryant of the U.S. Army Corps of the Engineers for the use of the model mangroves. USNA midshipmen McKenna Brophy, Jordan Keck, Dan McMann, and Nico Valdivieso and NHERI REU undergraduate researchers Alanna DaRin, Brenna Derby, and Grace Pond assisted with the experiments. The project was supported by funding from the National Science Foundation through Grants 2037914, 2110262, and 2110439 and the US Army Corps of Engineers through project number W912HZ2120045. Any opinions, findings, conclusions, or recommendations expressed in this material are those of the authors and do not necessarily reflect the views of the NSF, USACE, or USNA.

References

Ahrens, J. P., & Heimbaugh, M. S. (1988). Irregular Wave Runup on Riprap Revetments. *Journal of Waterway, Port, Coastal, and Ocean Engineering*, *114*(4), 524–530. https://doi.org/10.1061/(ASCE)0733-950X(1988)114:4(524)

Alongi, D. M. (2014). Carbon Cycling and Storage in Mangrove Forests. *Annual Review of Marine Science*, *6*(1), 195–219. https://doi.org/10.1146/annurev-marine-010213-135020

Bao, T. Q. (2011). Effect of mangrove forest structures on wave attenuation in coastal Vietnam. *Oceanologia*, *53*(3), 807–818. https://doi.org/10.5697/oc.53-3.807

Bridges, T., King, J., Simm, J., Beck, M., Collins, G., Lodder, Q., & Mohan, R. (2021). *International Guidelines on Natural and Nature-Based Features for Flood Risk Management*. Engineer Research and Development Center (U.S.). https://doi.org/10.21079/11681/41946

Bruce, T., van der Meer, J. W., Franco, L., & Pearson, J. M. (2009). Overtopping performance of different armour units for rubble mound breakwaters. *Coastal Engineering*, *56*(2), 166–179. https://doi.org/10.1016/j.coastaleng.2008.03.015

Bryant, M., Bryant, D., Provost, L., Hurst, N., McHugh, M., Wargula, A., & Tomiczek, T. (2022). *Wave attenuation of coastal mangroves at a near-prototype scale*. Engineer Research and Development Center (U.S.). https://doi.org/10.21079/11681/45565

Dalrymple, R. A., Kirby, J. T., & Hwang, P. A. (1984). Wave Diffraction Due to Areas of Energy Dissipation. *Journal of Waterway, Port, Coastal, and Ocean Engineering*, *110*(1), 67–79. https://doi.org/10.1061/(ASCE)0733-950X(1984)110:1(67)

Dawes, C., Siar, K., & Marlett, D. (1999). Mangrove structure, litter and macroalgal productivity in a northern-most forest of Florida. *Mangroves and Salt Marshes*, *3*, 259–267.

De Rouck, J., Verdonck, R., Troch, P., Van Damme, L., Schlütter, F., & De Ronde, J. (1999). Wave Run-Up and Overtopping: Prototype Versus Scale Models. *Coastal Engineering 1998*, 1039–1052. https://doi.org/10.1061/9780784404119.077

De Rouck, J., Verhaeghe, H., & Geeraerts, J. (2009). Crest level assessment of coastal structures—General overview. *Coastal Engineering*, *56*(2), 99–107. https://doi.org/10.1016/j.coastaleng.2008.03.014

DeYoe, H., Lonard, R. I., Judd, F. W., Stalter, R., & Feller, I. (2020). Biological Flora of the Tropical and Subtropical Intertidal Zone: Literature Review for Rhizophora mangle L. *Journal of Coastal Research*, *36*(4), 857. https://doi.org/10.2112/JCOASTRES-D-19-00088.1

Doyle, T. W., Smith, T. J., & Robblee, M. B. (1995). Wind Damage Effects of Hurricane Andrew on Mangrove Communities Along the Southwest Coast of Florida, USA. *Journal of Coastal Research*, 159–168.

Faunce, C. H., & Serafy, J. E. (2006). Mangroves as fish habitat: 50 years of field studies. *Marine Ecology Progress Series*, *318*, 1–18. https://doi.org/10.3354/meps318001

Franco, C., & Franco, L. (1999). Overtopping Formulas for Caisson Breakwaters with Nonbreaking 3D Waves. *Journal of Waterway, Port, Coastal, and Ocean Engineering*, *125*(2), 98–108. https://doi.org/10.1061/(ASCE)0733-950X(1999)125:2(98)

Frigaard, P., & Lykke Andersen, T. (2014). *Analysis of waves: Technical documentation for wavelab 3*. DCE Lecture Notes No. 33, Aalborg University, Denmark.

Goda, Y. (2010). *Random Seas and Design of Maritime Structures*. 3rd ed. World Scientific https://doi.org/ 10.1142/7425.

Guannel, G., Ruggiero, P., Faries, J., Arkema, K., Pinsky, M., Gelfenbaum, G., Guerry, A., & Kim, C.-K. (2015). Integrated modeling framework to quantify the coastal protection services supplied by vegetation. *Journal of Geophysical Research: Oceans*, *120*(1), 324–345. https://doi.org/10.1002/2014JC009821

Guannel, G., Arkema, K., Ruggiero, P., & Verutes, G. (2016). The Power of Three: Coral Reefs, Seagrasses and Mangroves Protect Coastal Regions and Increase Their Resilience. *PLOS ONE*, *11*(7), e0158094. https://doi.org/10.1371/journal.pone.0158094

He, F., Chen, J., & Jiang, C. (2019). Surface wave attenuation by vegetation with the stem, root and canopy. *Coastal Engineering*, *152*, 103509.

Herrera-Silveira, J., Teutli-Hernandez, C., Secaira-Fajardo, F., Braun, R., Bowman, J., Geselbracht, L., & Guerra Cano, L. (2022). Hurricane damages to mangrove forests and post-storm restoration techniques and costs. *The Nature Conservancy: Arlington, TX, USA*.

Jimenez, J. A., & Lugo, A. E. (1985). Tree Mortality in Mangrove Forests. *Biotropica*, *3*(17), 177–185.

Jo, J., Kim, S., Mori, N., & Mase, H. (2024). Combined storm surge and wave overtopping inundation based on fully coupled storm surge-wave-tide model. *Coastal Engineering*, *189*, 104448. https://doi.org/10.1016/j.coastaleng.2023.104448

Kathiresan, K., & Bingham, B. L. (2001). Biology of mangroves and mangrove Ecosystems. In *Advances in Marine Biology* (Vol. 40, pp. 81–251). Academic Press. https://doi.org/10.1016/S0065-2881(01)40003-4

Kelty, K., Tomiczek, T., Cox, D. T., Lomonaco, P., & Mitchell, W. (2022). Prototype-Scale Physical Model of Wave Attenuation Through a Mangrove Forest of Moderate Cross-Shore Thickness: LiDAR-Based Characterization and Reynolds Scaling for Engineering With Nature. *Frontiers in Marine Science*, *8*, 780946. https://doi.org/10.3389/fmars.2021.780946

Koosheh, A., Etemad-Shahidi, A., Cartwright, N., Tomlinson, R., & Van Gent, M. R. A. (2024). Wave overtopping layer thickness on the crest of rubble mound seawalls. *Coastal Engineering*, *188*, 104441. https://doi.org/10.1016/j.coastaleng.2023.104441

Libby, M., Tomiczek, T., Cox, D.T., & Lomonaco, P. (2024). Understanding Hybrid Green-Gray Coastal Infrastructure Processes and Performance Uncertainties for Flood Hazard Mitigation. *DesignSafe* (Seattle, WA: DesignSafe-CI). In preparation.

Loría-Naranjo, M., Samper-Villarreal, J., & Cortés, J. (2015). Structural complexity and species composition of Potrero Grande and Santa Elena mangrove forests in Santa Rosa National Park, North Pacific of Costa Rica. *Revista de Biología Tropical*, *62*(4), 33. https://doi.org/10.15517/rbt.v62i4.20030

Macintosh, P. D. J. (2005). *World Bank, ISME, cenTER Aarhus (2004). Principles for a Code of Conduct for the Management and Sustainable use of Mangrove Ecosystems.*

Maza, M., Adler, K., Ramos, D., Garcia, A. M., & Nepf, H. (2017). Velocity and Drag Evolution From the Leading Edge of a Model Mangrove Forest. *Journal of Geophysical Research: Oceans*, *122*(11), 9144–9159. https://doi.org/10.1002/2017JC012945

Maza, M., Lara, J. L., & Losada, I. J. (2019). Experimental analysis of wave attenuation and drag forces in a realistic fringe Rhizophora mangrove forest. *Advances in Water Resources*, *131*, 103376. https://doi.org/10.1016/j.advwatres.2019.07.006

Maza, M., Roldán, M., Lara, J. L., & Losada, I. J. (2022). Experimental analysis of hybrid solutions for coastal protection. *Coastal Engineering Proceedings*, *37*, Article 37. https://doi.org/10.9753/icce.v37.management.71

Mazda, Y., Magi, M., Kogo, M., & Hong, P. N. (1997). Mangroves as a coastal protection from waves in the Tong King delta, Vietnam. *Mangroves and Salt Marshes*, *1*(2), 127–135. https://doi.org/10.1023/A:1009928003700

Mazda, Y., Magi, M., Ikeda, Y., Kurokawa, T., & Asano, T. (2006). Wave reduction in a mangrove forest dominated by Sonneratia sp. *Wetlands Ecology and Management*, *14*(4), 365–378. https://doi.org/10.1007/s11273-005-5388-0

Meinert, P., Lykke Anderson, T., & Frigaard, P. (2017) *Awasys7 user manual.* Hydraulic and Coastal Engineering Laboratory, Aalborg University, Denmark.

Mendez, F. J., & Losada, I. J. (2004). An empirical model to estimate the propagation of random breaking and nonbreaking waves over vegetation fields. *Coastal Engineering*, *51*(2), 103–118. https://doi.org/10.1016/j.coastaleng.2003.11.003

Menéndez, P., Losada, I. J., Torres-Ortega, S., Narayan, S., & Beck, M. W. (2020). The Global Flood Protection Benefits of Mangroves. *Scientific Reports*, *10*(1), 4404. https://doi.org/10.1038/s41598-020-61136-6

Mitchell, W. T. (2021). *Effect of an Idealized Mangrove Forest of Moderate Cross-shore Width on Loads Measured on a Sheltered Structure and Comparison with Predicted Forces*. Oregon State University.

Montgomery, J. M., Bryan, K. R., Mullarney, J. C., & Horstman, E. M. (2019). Attenuation of Storm Surges by Coastal Mangroves. *Geophysical Research Letters*, *46*(5), 2680–2689. https://doi.org/10.1029/2018GL081636

Nagelkerken, I., Blaber, S. J. M., Bouillon, S., Green, P., Haywood, M., Kirton, L. G., Meynecke, J.-O., Pawlik, J., Penrose, H. M., Sasekumar, A., & Somerfield, P. J. (2008). The habitat function of mangroves for terrestrial and marine fauna: A review. *Aquatic Botany*, *89*(2), 155–185. https://doi.org/10.1016/j.aquabot.2007.12.007

Narayan, S., Beck, M. W., Reguero, B. G., Losada, I. J., Wesenbeeck, B. van, Pontee, N., Sanchirico, J. N., Ingram, J. C., Lange, G.-M., & Burks-Copes, K. A. (2016). The Effectiveness, Costs and Coastal Protection Benefits of Natural and Nature-Based Defences. *PLOS ONE*, *11*(5), e0154735. https://doi.org/10.1371/journal.pone.0154735

Novitzky, P. (2010). *Analysis of Mangrove Structure and Latitudinal Relationships on the Gulf Coast of Peninsular Florida* [MA Thesis]. University of South Florida.

Ohira, W., Honda, K., Nagai, M., & Ratanasuwan, A. (2013). Mangrove stilt root morphology modeling for estimating hydraulic drag in tsunami inundation simulation. *Trees*, *27*(1), 141–148. https://doi.org/10.1007/s00468-012-0782-8

Ostrow, K.S. (2023). *Performance-Based Design Methodology for Using Emergent Vegetation to Mitigate Wave Overtopping*. Oregon State University.

Ostrow, K., & Cox, D. (2024). Performance-Based Design Methodology for Nature-Based Solutions: Application to Using Mangroves to Mitigate Wave Overtopping. Submitted to *Coastal Engineering*.

Pranchai, A. (2017). “Regeneration and Self-Thinning Processes in a Restored Rhizophora Apiculata Plantation in Southern Thailand.” *Agriculture and Natural Resources, 51*(5), 390–94. https://doi.org/10.1016/j.anres.2017.11.004.

Schoonees, T., Kerpen, N. B., & Schlurmann, T. (2021). Full-scale experimental study on wave overtopping at stepped revetments. *Coastal Engineering*, *167*, 103887. https://doi.org/10.1016/j.coastaleng.2021.103887

Sippo, J. Z., Lovelock, C. E., Santos, I. R., Sanders, C. J., & Maher, D. T. (2018). Mangrove mortality in a changing climate: An overview. *Estuarine, Coastal and Shelf Science*, *215*, 241–249. https://doi.org/10.1016/j.ecss.2018.10.011

Taillardat, P., Friess, D. A., & Lupascu, M. (2018). Mangrove blue carbon strategies for climate change mitigation are most effective at the national scale. *Biology Letters*, *14*(10), 20180251. https://doi.org/10.1098/rsbl.2018.0251

Tomiczek, T., O’Donnell, K., Furman, K., Webbmartin, B., & Scyphers, S. (2020a). Rapid Damage Assessments of Shorelines and Structures in the Florida Keys after Hurricane Irma. *Natural Hazards Review*, *21*(1), 05019006. https://doi.org/10.1061/(ASCE)NH.1527-6996.0000349

Tomiczek, T., Wargula, A., Lomónaco, P., Goodwin, S., Cox, D., Kennedy, A., & Lynett, P. (2020b). Physical model investigation of mid-scale mangrove effects on flow hydrodynamics and pressures and loads in the built environment. *Coastal Engineering*, *162*, 103791. https://doi.org/10.1016/j.coastaleng.2020.103791

Tomiczek, T., Mitchell, W.T., Lomónaco, P., Cox, D.T., and Kelty, K. (2024). “Prototype-scale Laboratory Observations of Wave Force Reduction by an Idealized Mangrove Forest of Moderate Cross-shore Width.” *Ocean Engineering, 310 (2),* 118740. https://doi.org/10.1016/j.oceaneng.2024.118740

U.S. Army Corps of Engineers. (2002). *CEM: Coastal Engineering Manual*. U.S. Army Corps of Engineers.

van Dang, H., Park, H., Shin, S., Tomiczek, T., Cox, D. T., Lee, E., Lee, D., & Lomonaco, P. (2023). Physical model comparison of gray and green mitigation alternatives for flooding and wave force reduction in an idealized urban coastal environment. *Coastal Engineering*, *184*, 104339. https://doi.org/10.1016/j.coastaleng.2023.104339

van der Meer, J., Allsop, W., Bruce, T., Rouck, J., Kortenhaus, A., Pullen, T., Schüttrumpf, H., Troch, P., & Zanuttigh, B. (2018). *EurOtop: Manual on wave overtopping of sea defences and related sturctures—An overtopping manual largely based on European research, but for worlwide application (2nd edition)*.

Wu, W.-C., & Cox, D. T. (2015). Effects of wave steepness and relative water depth on wave attenuation by emergent vegetation. *Estuarine, Coastal and Shelf Science*, *164*, 443–450. https://doi.org/10.1016/j.ecss.2015.08.009

Zelt, J. A., & Skjelbreia, J. E. (2015). *Estimating Incident and Reflected Wave Fields Using an Arbitrary Number of Wave Gauges*. 777–789. https://doi.org/10.1061/9780872629332.058

Zhang, Y., Yang, Y., Yang, K., Tan, X., Sun, X., Leng, B., Zhou, C., & Zhu, B. (2020). Non-linear wave attenuation quantification model improves the estimation of wave attenuation efficiency of mangroves. *Estuarine, Coastal and Shelf Science*, *245*, 106927

Zhao, C., Tang, J., & Shen, Y. (2022). Numerical investigation of the effects of rigid emergent vegetation on wave runup and overtopping. *Ocean Engineering*, *264*, 112502. https://doi.org/10.1016/j.oceaneng.2022.112502

Appendix A: Development of equations predicting reduction in overtopping discharge

The proportional reduction in discharge is defined according to equation (A1), where δ_i is the proportional reduction from the discharge over the unprotected wall q_W to the discharge over the wall with any protective configuration q_i:

$$\delta_i = \frac{q_W - q_i}{q_W} \tag{A1}$$

We can write equation (A1) for a revetment (A2), a mangrove forest of density *2N* (A3), and a hybrid system with a revetment and a mangrove forest (A4):

$$\delta_R = \frac{q_W - q_R}{q_W} \tag{A2}$$

$$\delta_{2N} = \frac{q_W - q_{2N}}{q_W} \tag{A3}$$

$$\delta_{R+2N} = \frac{q_W - q_{R+2N}}{q_W} \tag{A4}$$

Note that although the *2N* forest is assumed in this derivation, the definitions of equations (A3) and (A4) are not specific to any forest density, and the subscript *2N* could be replaced by any other forest density without affecting the derivation.

We assume that the reduction in discharge due to a hybrid configuration with non-interacting revetment and mangrove forest components could be calculated as the sum of the reduction from each component minus the "double-counting" effect of interaction:

$$\delta_{R+2N} = \delta_R + \delta_{2N} - \delta_R\delta_{2N} \tag{A5}$$

We solve equation (A4) for the expected discharge rate over the hybrid system:

$$q_{R+2N} = q_W - \delta_{R+2N}q_W \tag{A6}$$

And substitute equation (A5) for the proportional reduction term:

$$q_{R+2N} = q_W - (\delta_R + \delta_{2N} - \delta_R\delta_{2N})q_W \tag{A7}$$

We solve equation (A2) to isolate the expected discharge rate over the revetment:

$$q_R = q_W - \delta_R q_W \tag{A8}$$

We combine equation (A7) and equation (A8) to calculate the proportional reduction by mangroves of the discharge over the revetment:

$$\frac{q_R - q_{R+2N}}{q_R} = \frac{(q_W - \delta_R\, q_W) - (q_W - (\delta_R + \delta_{2N} - \delta_R\delta_{2N})q_W)}{q_W - \delta_R\, q_W} \tag{A9}$$

We simplify the RHS of equation (A9):

$$\frac{q_R - q_{R+2N}}{q_R} = \frac{\delta_{2N} - \delta_R\delta_{2N}}{1 - \delta_R} = \delta_{2N} \tag{A10}$$

And substitute equation (A3) for the RHS of equation (A10):

$$\frac{q_R - q_{R+2N}}{q_R} = \frac{q_W - q_{2N}}{q_W} \tag{A11}$$

Equation (A11) is identical to equation (4) in section 4.2 of this paper.

We can then adjust equation (A5) by including reduction by a correction factor δ_{CF}:

$$\delta_{R+2N} = \delta_R + \delta_{2N} - (\delta_R \delta_{2N} - \delta_{CF}) \tag{A12}$$

And substitute into equation (A6) to obtain:

$$q_{R+2N} = q_W - (\delta_R + \delta_{2N} - (\delta_R \delta_{2N} - \delta_{CF}))q_W \tag{A13}$$

Then combine equation (A8) with the new equation (A13) to calculate the proportional reduction by mangroves of the discharge over the revetment, considering the correction factor:

$$\frac{q_R - q_{R+2N}}{q_R} = \frac{(q_W - \delta_R\, q_W) - (q_W - (\delta_R + \delta_{2N} - (\delta_R \delta_{2N} - \delta_{CF}))q_W)}{q_W - \delta_R\, q_W} \tag{A14}$$

We can simplify the RHS of equation (A14):

$$\frac{q_R - q_{R+2N}}{q_R} = \frac{\delta_{2N} - \delta_R \delta_{2N} + \delta_{CF}}{1 - \delta_R} = \delta_{2N} + \frac{\delta_{CF}}{1 - \delta_R} \tag{A15}$$

And substitute equation (A3):

$$\frac{q_R - q_{R+2N}}{q_R} = \frac{q_W - q_{2N}}{q_W} + \frac{\delta_{CF}}{1 - \delta_R} \tag{A16}$$

Equation (A16) is identical to equation (5) in section 4.2 of this paper.